COMBUSTION INSTABILITIES IN NON-PREMIXED

OPPOSED-FLOW TUBULAR FLAMES

By

Scott William Shopoff

Thesis

Submitted to the Faculty of the

Graduate School of Vanderbilt University

in partial fulfillment of the requirements

for the degree of

MASTER OF SCIENCE

in

Mechanical Engineering

December, 2010

Nashville, Tennessee

Approved:

Professor Robert. W. Pitz

Professor Deyu Li

Professor Amrutur V. Anilkumar

ACKNOWLEDGEMENTS

TABLE OF CONTENTS

Chapter

LIST OF TABLES

LIST OF FIGURES

LIST OF SYMBOLS

A area

AJ   axisymmetric jet

c_p specific heat of constant pressure

CFD   computational fluid dynamics

D   mass diffusivity of the gas

Da   Damköhler number

K   stretch rate

Ka   Karlovitz number (non-dimensional stretch rate)

Le   Lewis number

$\vec{n}$ unit normal vector of the flame surface

NPOF non-premixed opposed-flow

$\sqrt{Q}$ normalized pressure eigenvalue

R_i radius of nozzle ('i' is 1 for inner nozzle and 2 for outer nozzle)

R_s stagnation radius

$S_f^{\;o}$ adiabatic flame speed

t time

T   temperature

U_z velocity in the axial direction

v_n normal component of the velocity of the flame surface (flame surface speed)

$\vec{V}$ local fluid velocity

V_i velocity at nozzle exit ('i' is 1 for inner nozzle and 2 for outer nozzle)

WP   Wolfhard-Parker

Z   axial direction of the burner

λ thermal conductivity

α thermal diffusivity

ρ_i density of the gas ('i' is 1 for inner nozzle and 2 for outer nozzle)

Φ initial mixture strength

δ diffusion length or flame thickness

ξ_{st} stoichiometric mixture fraction

ABSTRACT

Cellular formation in non-premixed flames is experimentally studied in an opposed-flow tubular burner that allows independent variation of the global stretch rate and overall flame curvature. All experiments were conducted burning H_2 diluted with CO_2 flowing against air. The transitions to cellularity, cellular structures, and extinction conditions were determined as a function of the initial mixture strength, stretch rate, and curvature. The progression of cellular formation from the onset of cells through extinction was analyzed in the tubular burner by flame imaging using an intensified CCD camera. Cells formed near extinction at low fuel Lewis numbers and low initial mixture strengths. The experimental onset of cellular instability is found to be at or slightly above the numerically determined 1D tubular flame extinction limit.

For fuel Lewis numbers less than unity, concave curvature towards the fuel retards combustion and weakens the flame and convex curvature towards the fuel promotes combustion and strengthens the flame. In the cell formation process, the concave flame cell midsection is weakened and the convex flame cell ends are strengthened. With increasing stretch rate, the flame thickness at the cell midsection decreases while the flame thickness of the cell edges is unchanged, with further increase in stretch rate, the flame breaks into cells and the cell formation process continues until near-circular cells are formed with no concave midsection. Further increase in the stretch rate leads to cell extinction. The results show the importance of local flame curvature in the formation of flame cells.

To assess hysteresis effects, three different procedures of decreasing the Damköhler number (positive process), as well as using those same procedures in the opposite progression of increasing the Damköhler number (negative process) were completed. Significant flame hysteresis was seen and the positive transition occurred at a lower Damköhler number than the negative transition.

Mechanical perturbations were conducted to show that the onset of cellularity could be realized at a higher Damköhler number. Once cellular instability was induced, it was possible to perturb the flame into multiple stable cellular states and extinguish the flame at a much higher Damköhler number than without perturbations. Images are shown of rotating cellular flames and a cellular instability regime at an initial mixture strength greater than unity and away from extinction conditions. A qualitative explanation of flame rotation and a general categorizing of three distinct flame regimes are given.

THESIS ORGANIZATION

The thesis is broken down into three sections. The first section (CHAPTER I and II) gives an overview of previous cellular instability experiments in both premixed and non-premixed flames and presents a background into the present efforts to better understand this type of combustion phenomenon. The focus of this thesis is on non-premixed combustion, especially in the non-premixed opposed-flow tubular burner at Vanderbilt University. This section describes the efforts to better understand combustion in this burner and relate it to overall combustion mechanisms.

The second section (CHAPTER III, IV, and V) gives a thorough explanation of the non-premixed opposed-flow tubular burner and describes how it is able to quantify and qualify the stretch rate, flame curvature, and preferential diffusion in non-premixed combustion. The second section also goes into detail on the procedures used to test these flame parameters, describes the results of these tests, and discusses the significance of the results.

Finally, the third section (CHAPTER VI) reviews the findings of the second section and ties those findings into what was already known about combustion from the first section. A discussion on future efforts and experiments that can still be run in the non-premixed opposed-flow tubular burner or other burners that would lead future researchers to a better understanding of combustion in general is presented too.

CHAPTER I

INTRODUCTION

Motivation

With the advance of computational fluid dynamics (CFD) and the availability of high speed computer modeling, combustion researchers are continuously striving to model flames numerically. In order for these simulations to be useful, it is crucial that they accurately reflect the actual real world flames. Key areas of research in combustion modeling are the ability to model flame instabilities and turbulence. In turbulent combustion, the laminar flamelet model plays an important role (Peters, 1984). This model uses the fact that the reaction zone of a flame is very thin and even in high turbulence the flow does not alter the flame's structure more than if it were a laminar flame subjected to the same scalar dissipation. The underlying concept is that the turbulent flame can be modeled as an ensemble of laminar flamelets. The success of the laminar flamelet model has been the ability of combustion researchers to replicate laminar flamelets of interest in non-turbulent flows and then to add this information to the library of combustion modeling. In order to replicate these laminar flamelets, unique burners need to be developed.

There are two different types of non-premixed burners. A parallel type [e.g. Burke-Schumann and Wolfhard-Parker (WP) burner] in which a diffusion flame is established between two parallel streams of fuel and oxidizer, and a counterflow type (e.g. planar and tubular burner) in which a diffusion flame is established between two

opposing streams of fuel and oxidizer. The counterflow burner is more "purely" diffusional because parallel type burners allow for some premixing along the boundary layer of the burner walls that initially separate the reactants at the burner exit. This is best seen in Lo Jacono and Monkewitz (2007), where the authors used the jet shear layer and vorticity thickness in their Axisymmetric Jet (AJ) burner to calculate the wavelength of cellular instability. In this thesis, the tubular burner is used to model the flames of interest.

The three main parameters of any flame are the flame temperature, the flame speed, and the stretch rate; without understanding all three of them it is impossible to understand what is happening in and around the reaction zone. The flame temperature is a value associated with how hot the flame is. It is such a widely used and easily understood term, more detail is not given.

Flame speed is a much more complicated parameter. Flame speed involves the expansion of the flame front, the interplay of the premixing fuel and oxidizer, and both the upstream (unburned) and downstream (burned) conditions. In non-premixed combustion there exists no flame speed. Non-premixed combustion has no mixing of fuel and oxidizer before the flame, therefore the flame is restricted to a small reaction zone whose size and shape is dependent on the diffusion of the fuel and oxidizer. In the non-premixed opposed-flow tubular burner of this study, the flame speed is replaced by the flame curvature. The flame curvature describes the geometry of the flame sheet. The curvature is the inverse of the stagnation radius (or flame radius). This is a very important factor and its effects are seen on all other flame parameters. From this point on, 'NPOF' will replace 'non-premixed opposed-flow'.

The last flame parameter is the stretch rate, which is the most complicated of the three parameters. The stretch rate will be seen to greatly affect the flame temperature and will be seen to be greatly affected by the flame curvature. The stretch rate is manifested by the flame's geometry, the flow's non-uniformity, and the flame's motion. It is defined as the non-dimensional rate of flame area change, $K = \dfrac{1}{A}\dfrac{dA}{dt}$. It influences the tangential and normal velocity gradients and the flame adjusts its location in response to stretch in order to maintain a high temperature and low reactant leakage. From this point on, the term 'stretch rate' and 'stretch' will be interchangeable and mean the same thing.

The goal of the present thesis is to perform a detailed and systematic experimental investigation of a stretched, curved diffusion flame burning hydrogen diluted with carbon dioxide flowing against air in the NPOF tubular burner. The flame was imaged using a high resolution ICCD camera. It records a much more detailed image of the flame compared to the previous cameras used at Vanderbilt University (Hu et al., 2009a; Wang et al., 2009). It has the capability to record a numeric value for the chemiluminescence that can quantify the burning intensity at any spectral location as well as zooming into regions of greater interest for more thorough investigation. It is optimal for studying the cellular instabilities in this burner. Laser diagnostic techniques have not been used to study cellular instabilities in the NPOF tubular burner, physical probes affect the flow in the vicinity of the cellular instabilities, and currently numerical simulations cannot accurately predict the complex 3-D structures associated with cellular instabilities. Therefore at the present time, this camera serves as the best means to accurately quantify and qualify cellular instabilities in the NPOF tubular burner.

Hydrogen has been chosen as the fuel for this study for two reasons. The first and most important reason is that hydrogen has a large mass difference compared to other hydrocarbons and inert diluents. This produces interesting non-equidiffusive effects (i.e. preferential and differential diffusion). Secondly, hydrogen has been proposed as an important alternative fuel source for the future. Hydrogen combustion has been proposed as an alternative fuel source because of its low pollutant production, high temperature, and high energy density. Hydrogen was diluted with carbon dioxide which negates the low pollution and clean burning. Carbon dioxide was chosen because of the large mass difference compared to hydrogen and because it is chemically inert in these applications. It could be replaced by nitrogen with very similar outcomes, which was shown in Hu et al. (2009a).

Previous Work

Two very important qualities of flames in the laminar flamelet library (Peters, 1984) are stretch and curvature. Stretch has been modeled in many burner configurations by several researchers. Law (1988) and Matalon (1983) have both written extensive reviews on the subject. Curvature is more difficult to model accurately, especially as it relates to flame instability. One of the best ways to model flame curvature is the use of a tubular burner.

One of the earliest and most comprehensive studies on tubular flames was by Ishizuka (1993) (this work mainly concerns itself with premixed combustion, but so does most experimental combustion work). Ishizuka studied stretched, curved flames in a

rotating and non-rotating axisymmetric flow field. In turbulent flows, flames are usually subjected to coupled motions of stretch and rotation.

In his study, Ishizuka (1993) found that the stability limits of tubular flames in a rotating and non-rotating flow field are strongly influenced by the Lewis number of the limiting reactant in the mixture. He found that in lean H_2/air flames the flame temperature can be raised and the flammability limit can be extended if the flow field was rotating as opposed to non-rotating. It was even shown that increasing the intensity of rotation extended the flammability limit further. This phenomenon was attributed to the transport of hydrogen into the reaction zone by preferential diffusion during rotation. It was shown by Wang et al. (2006) that rotation does not essentially alter the tubular flame structure or flow field compared to a non-rotating flow.

In a first study on tubular flames at Vanderbilt, Wang et al. (2006) analytically solved for the flow field of the opposed tubular burner. The focus of the study was solving for the stretch rate and stagnation radius of the flames. In order to accurately compare the effects of curvature on the properties of stretched flames, comparisons of tubular and planar diffusion flames must be based on the same stretch rate. It was shown that the analytical results of the flame stretch and radius agreed well with numerical solutions. The peak stretch rate occurred in a large enough region and wasn't fluctuating enough in that region to use the analytical equations to solve for the tubular burner's flow field.

In a follow-up study, Wang et al. (2007) numerically compared the tubular diffusion flame to the planar diffusion flame to show the effect of curvature on preferential diffusion. It was shown that positive curvature (convex curvature to the fuel)

strengthens preferential diffusion and negative curvature (concave curvature to the fuel) weakens preferential diffusion. When the Lewis number of the fuel is less than unity increased preferential diffusion leads to higher temperatures and stronger flames. The opposite is true of flames with a Lewis number of the fuel greater than unity. The strengthening or weakening of the flame was shown to be proportional to the ratio of the flame thickness to flame radius.

In the first experimental study on non-premixed tubular flames, Hu et al. (2007) used Raman scattering to obtain values of species concentrations and flame temperatures in H_2 diluted with N_2 versus air flames at varying stretch rates. In the study, three important experimental realizations were accomplished: i. measured temperature and specie concentrations agreed well with numerical predictions (but only at moderate stretch rates); ii. concave (convex) curvature weakens (strengthens) preferential diffusion for flames and when the Lewis number of the fuel is less than unity this leads to higher (lower) flame temperatures (more than unity); and iii. cellular instabilities were observed at high stretch rates, near extinction.

Later, Hu et al. (2009a) burned H_2 diluted with N_2, He, Ar, and CO_2 versus air in a tubular burner. It was found that cellular instability was realized with all diluents except helium. This was attributed to the fact that when the fuel was diluted with helium the Lewis number was very near unity (Le_{fuel}= ~1.09-1.1). Therefore there existed very little preferential diffusion. Cellular instability was observed when the fuel was introduced from the inner nozzle and oxidizer from the outer nozzle and vice versa. Lastly, the cellular regime was mapped from the condition at the onset of cellularity until extinction using the initial mixture strength, stretch rate, and flame curvature

<u>Present Work</u>

In Hu et al. (2007), experimental results were compared to numerical simulations to assess their accuracy. It was found that the numerical simulations were unable to accurately predict the extinction stretch rate or the existence of cellular structures. It was feasible for the numerical simulations to predict these values for curved, stretched flames when the Lewis number was roughly equal to unity because those flames had no preferential diffusion or preference of curvature. Due to heat loss to the inner nozzle at low stretch rates and to cellular structures at high stretch rates, the experimental results were only accurate for moderate stretch rates. In Hu et al. (2009a), the values of the stretch rate, initial mixture strength, and curvature were measured from the onset of cellularity until extinction. In the study, no flame images were shown and no temperature or major species concentrations were measured.

This present study fills in the gaps by displaying the flame images and complicated three-dimensional geometry of the cellular instabilities not seen earlier. This study takes advantage of the new ICCD camera to show the difference in burning intensity at different locations along the reaction zone. Also this study offers new comparisons between curved, stretched diffusion flames and planar, stretched diffusion flames. Clear images of the transition of a noncellular flame to cellular and then to extinction, systematic categorization of two different cellular flame regimes, and a discussion on flame rotation are also included.

The fuel of this study was always H_2 diluted with CO_2 and the oxidizer was always air. The transitions to cellularity, cellular structures, and extinction conditions are determined as a function of the initial mixture strength, stretch rate, and curvature. The

experimental onset of cellular instability is found to be at or at a slightly lower Damköhler number than the numerically determined 1D tubular flame extinction limit. The experimental limits of the onset of cellular instability and extinction are compared by lowering the initial mixture strength or increasing the stretch rate. Three different procedures of flame progression towards extinction were used (called the positive process). Oppositely, the negative process (i.e. progressing the flame from near extinction until a noncellular flame was re-established) of these three procedures was conducted to show flame hysteresis. Prior experimental and numerical studies have focused on the progression of flames towards extinction; in this study, the opposite process of going from near extinction to a noncellular flame is conducted. Lastly, mechanical perturbations to the flow were employed to show the effects of flame perturbations on the onset of cellularity and extinction and the possibility of having multiple stable cellular states at the same flow condition.

It was shown that while cells are forming, the concave midsection of the flame is weaker than the convex flame edge. Approaching extinction, the flame breaks into cells and cell formation continues until circular cells with no concave midsection are observed. Further decrease in Damköhler number leads to extinction. With increasing stretch rate, the flame thickness at the cell midsection decreases similar to the planar opposed-flow flame while the thickness of the flame edges are unchanged and can even increase due to the strengthening effects of convex curvature. The results show the importance of local flame curvature in the formation of flame cells and in the existence of cellular flames well beyond the 1D extinction limit.

CHAPTER II

THEORETICAL REVIEW

Cellular Instabilities

Instability phenomena have been observed by many researchers using different non-premixed burners and under various experimental conditions. With a slot burner, Chen et al. (1992) proposed that non-premixed flames with sufficiently low reactant Lewis numbers exhibit cellular instability only near extinction. Lo Jacono et al. (2003) studied an AJ flame burning H_2 in O_2 with both streams diluted by CO_2. They found that at low reactant Lewis numbers and near extinction conditions cellular structures could be formed and that these structures showed a strong dependency on the initial mixture strength, Φ (the ratio of fuel mole fraction in the fuel stream to oxidizer mole fraction in the oxidizer stream normalized by the stoichiometric fuel-to-oxidizer molar ratio). Using the same AJ burner and a WP slot burner, Lo Jacono and Monkewitz (2007) found multiplicity of the cellular states and calculated the cell wavelength as a function of the fuel jet velocity and initial mixture strength. Lo Jacono et al. (2005) constructed a new unstrained[1] planar non-premixed burner and confirmed that cellular instability is more prevalent at low initial mixture strengths and low Damköhler numbers (the ratio of the characteristic flow time to the characteristic chemical time). With an improved unstrained planar non-premixed burner, Robert and Monkewitz (2009) found that the cell size scaled with the inverse of the flow velocity; this confirmed previous stability analyses

---

[1] Flame strain and flame stretch have been used interchangeably in the past to mean the same thing. Further detail is given in CHAPTER II. Stretch and Curvature in Flames.

(Cheatham and Matalon, 2000; Kim et al., 1996). Lee and Kim (2002) numerically simulated flames in an opposed jet burner and observed the sublimit nature of the cellular flame (i.e. cellular flames existed with Damköhler numbers much less than the 1D critical extinction value). Instabilities in premixed and non-premixed flames have also been thoroughly reviewed by Matalon (2007; 2009).

As can be seen, experimental and numerical studies of cellular instabilities in diffusion flames have been performed in many different burners and under various conditions. The underlying similarities between all these experiments is that cellular instabilities occur at low reactant Lewis numbers and low Damköhler numbers with an emphasis on heavily diluted fuels. In a NPOF tubular flame, the cellular structures can be studied under conditions of constant curvature, initial mixture strength, and stretch rate and these parameters can be varied one at a time. This makes this burner very attractive for conducting experiments.

The two most important parameters leading to cellular instability are the preferential diffusion (Lewis number) and near extinction conditions (Damköhler number). Chen et al. (1992) obtained cellular instabilities at greater than unity initial mixture strengths but not at near unity Lewis numbers. Preferential diffusion is based on a difference in the heat and mass diffusion. Whether $Le \neq 1$ or $Le=1$, corresponds to if preferential diffusion exists or not, respectively. The Lewis number is defined as the ratio of the thermal diffusivity to the mass diffusivity and can be seen in Equation (1). In the case of non-premixed flames, there exist two Lewis numbers. The Lewis number of the fuel and the Lewis number of the oxidizer. To complicate things, because the fuel is diluted; the Lewis number of the fuel is the ratio of the thermal diffusivity of the bulk

mixture (in this study H_2 and CO_2) to the mass diffusivity of the deficient reactant (in this study H_2).

$$Le = \frac{\lambda}{c_p \rho D} = \frac{\alpha}{D} \tag{1}$$

In an early study on tubular flame instabilities in a non-rotating, axisymmetric flow field, Ishizuka (1993) found that when buoyancy was in the direction perpendicular to the axis of symmetry, a denting of the bottom of the flame occurred. It was found that this deformation occurred when the Lewis number of the deficient reactant was less than unity and at lean fuel conditions. When the buoyancy was in the direction parallel to the axis of symmetry, a cellular pattern appeared when the Lewis number of the deficient reactant was less than unity and at lean fuel conditions.

In two important experimental studies at Vanderbilt in the NPOF tubular burner, Hu et al. (2007; 2009a) was able to show that lean hydrogen flames with Lewis numbers less than unity formed cellular structures. These structures could change orientation from concave to convex curvature at high stretch rates.

In all flames regardless of being premixed or non-premixed, at near extinction conditions either the flame will become fully quenched or display interesting instability phenomenon. In this study, instability is manifested as cellular structures. In all experiments, the Lewis number of the deficient reactant was the driving force behind these cellular instabilities (Chen et al., 1992; Hu et al., 2007; Ishizuka, 1993; Lo Jacono et al., 2003; Matalon, 2007). Because there is much debate over the correct nomenclature between preferential diffusion and differential diffusion: preferential diffusion will be defined in this manuscript as the effect of the Lewis number (the ratio of the thermal

11

diffusivity versus the molecular diffusivity); differential diffusion will be defined as the difference in molecular diffusivity of each specific chemical molecule (i.e. D_{CO_2} versus D_{H_2}).

In the case of this manuscript, all flames were lean with the fuel being hydrogen diluted with carbon dioxide. The high stretch rates cause the hydrogen to diffuse to the reaction zone faster and in larger quantities than the carbon dioxide (differential diffusion) and the diffusion of un-reacted hydrogen exceeds the heat loss of the reactions (preferential diffusion). Increasing the stretch rate or lowering the initial mixture strength creates local regions of the flame with very high temperatures. High temperature means high reaction rates. As the flame progresses towards extinction, these local regions of high reactivity resist extinction and lead to cellular instabilities. The cellular instability is mainly affected by the diffusion of the deficient reactant (hydrogen). This is possible because all of these flames are far from the stoichiometric condition and therefore the availability and mobility of the deficient reactant controls the flame characteristics.

Stretch and Curvature in Flames

Stretch is a manifestation of three factors: the existence of flame curvature, the flow of reactants parallel to the reaction zone, and the flow of reactants normal to the reaction zone (Law, 1988). Flame stretch can be present if one or all three of the previous factors occur. The influences of stretch are on the tangential and normal velocity gradients of the reactants. The combined effects of these gradients are to displace the flame surface (only applicable in un-restrained flames), distort the topography (winkled flames), and modify the volumetric burning rate (differences in flame temperature above

or below the adiabatic flame temperature). In an un-restrained flame (mainly premixed), the flame can freely adjust its location in response to stretch in order to achieve a more complete reaction. Therefore stretch has a minimal effect on these flames. In NPOF tubular flames, the flame is curved by the shape of the burner, non-equidiffusive because of the dilution of the reactants, and restrained by the stagnation surface. When the flame is curved, non-equidiffusive, and restrained, stretch has a great affect on other flame parameters.

A lot of combustion research uses the terms flame "strain" and flame "stretch" interchangeably. In this thesis, the term flame stretch will be used. Flame stretch is a combination of three things: flame straining (flow non-uniformity tangential to the flame surface), flame curvature, and flame motion (flow non-uniformity normal to the flame surface). It is the opinion of the author that flame strain does not give the full meaning of the term as it pertains to this burner because of the significant influence of curvature on the flame's geometry. Therefore stretch is used.

Karlovitz (1953) first introduced the concept of flame stretch, K. He used it to explain flame extinction in velocity gradients. He defined stretch as a quantity having both a location and time and changing along the flame front and over time. Along a continuous flame front there may exist points with K<0 (negative stretch), K>0 (positive stretch), and K=0 (stretchless flames).

Williams (1975) defined a non-dimensional stretch rate analytically called the Karlovitz number and solved for the expression:

$$Ka = \frac{\delta}{S_f^{\,0}}(K)$$

(2)

Equation (2) is for premixed flames with S_f^0 being the adiabatic flame speed. For non-premixed flames (that do not have a flame speed) the dimensional stretch rate is used:

$$K = \frac{1}{A}\frac{dA}{dt} \tag{3}$$

A is the area of points that stay on the flame surface because they have the same normal velocity as the flame surface, and also have the same tangential velocity as nearby fluid particles. Both Equations (2) and (3) are general expressions for stretch but would be more useful if they depended on measurable flame quantities. Therefore, Matalon (1983) derived a general formula for flame stretch as:

$$Ka = \frac{\delta}{S_f^o}(-curl(\vec{V}\times\vec{n})_{F=0}\cdot\vec{n} + v_n div\,\vec{n})_{F=0} \tag{4}$$

$$K = (-curl(\vec{V}\times\vec{n})_{F=0}\cdot\vec{n} + v_n div\,\vec{n})_{F=0} \tag{5}$$

Equation (4) is for premixed and Equation (5) can be used for non-premixed flames. In Equations (4) and (5), the first term results from the non-uniform flow field across the curved front and the second term results from the motion of the moving curved front (Matalon, 1983). Therefore, it is possible for a flame in a uniform flow field ($curl(\vec{V}\times\vec{n})_{F=0}\cdot\vec{n} = 0$) to experience stretch because of the normal velocity and curvature at a specific location. Also, a stationary flame ($v_n div\,\vec{n} = 0$) can experience stretch because of nonuniform flow of reactants and curvature.

The stretch rate is a very important flame parameter and affects the flame speed, temperature, and thickness (Matalon, 1983; Law, 1988; Sung et al., 1995). Wang et al.

14

(2006) used the definition of stretch as given by Williams (1975) [Equation (3)] and Matalon (1983) [Equation (5)] to derive the stretch rate for the NPOF tubular burner. The stretch rate includes two parts Matalon (1983): the local fluid velocity normal to the flame and the flame surface speed relative to the tangential motion. Wang re-arranged Equation 5 to: $K = -[\nabla \times (\vec{V} \times \vec{n})] \cdot \vec{n} + v_n (\nabla \cdot \vec{n})$, where $\vec{V}$ is the local fluid velocity, $\vec{n}$ is the unit normal vector of the flame surface, v_n is the normal component of the velocity of the flame surface (flame surface speed), $\nabla \cdot \vec{n}$ is the flame curvature, and $-[\nabla \times (\vec{V} \times \vec{n})] \cdot \vec{n}$ is the flow field and flame shape. For a steady flame, $v_n = 0$, and the stretch rate just depends on flow field and flame shape.

From Williams (1975), Wang et al. (2006) solved Equation (3) by evaluating $K = \frac{1}{A}\frac{dA}{dt} = \frac{\partial U_z}{\partial Z}$. Where U_z is the velocity in the axial direction 'Z'. The stretch rate for a planar diffusion flame was already accomplished (Seshadri and Williams, 1978), therefore Wang et al. (2006) analytically solved the stretch rate of the NPOF tubular flame and determined the expressions for each side of the stagnation surface. In this study, the reaction zone is near the stagnation surface. Based on Wang's analytical solution (2006), the stretch rate at the stagnation surface is as follows:

Side 2 (outer nozzle side) of the stagnation surface: $K = \dfrac{-V_2 \sqrt{Q}}{R_2}$ (6)

Side 1 (inner nozzle side) of the stagnation surface: $K = \dfrac{-V_2 \sqrt{\dfrac{\rho_2}{\rho_1} Q}}{R_2}$ (7)

$$\sqrt{Q} = \pi \left(\frac{\dfrac{R_2}{R_1} - \sqrt{\dfrac{\rho_1}{\rho_2}\dfrac{V_1}{V_2}}}{\dfrac{R_2}{R_1} - \dfrac{R_1}{R_2}} \right) \tag{8}$$

Multiplying both the numerator and denominator of Equation (8) by $\sqrt{\dfrac{\rho_2}{\rho_1}\dfrac{V_2}{V_1}}$ yields

$$\sqrt{Q} = \pi \left(\frac{\dfrac{R_2}{R_1} - \sqrt{\dfrac{\rho_1}{\rho_2}\dfrac{V_1}{V_2}}}{\dfrac{R_2}{R_1} - \dfrac{R_1}{R_2}} \right) \cdot \frac{\sqrt{\dfrac{\rho_2}{\rho_1}\dfrac{V_2}{V_1}}}{\sqrt{\dfrac{\rho_2}{\rho_1}\dfrac{V_2}{V_1}}} \tag{9}$$

Re-arranging yields:

$$\sqrt{Q} = \frac{\pi}{\sqrt{\dfrac{\rho_2}{\rho_1}\dfrac{V_2}{V_1}}} \left(\frac{\dfrac{V_2}{V_1}\dfrac{R_2}{R_1}\sqrt{\dfrac{\rho_2}{\rho_1}} - 1}{\dfrac{R_2}{R_1} - \dfrac{R_1}{R_2}} \right) \tag{10}$$

Since air is the oxidizer and there is little preferential diffusion on the oxidizer side ($Le_{oxidizer} = \sim1$), the stretch rate is given based on the fuel side of the stagnation surface. In this study, the fuel is always issued from the inner porous nozzle (side 1), so the stretch rate is given by Equation (7). Applying Equation (10) into Equation (7):

$$K = \frac{-V_2\sqrt{\dfrac{\rho_2}{\rho_1}}}{R_2} \frac{\pi}{\sqrt{\dfrac{\rho_2}{\rho_1}\dfrac{V_2}{V_1}}} \left(\frac{\dfrac{V_2}{V_1}\dfrac{R_2}{R_1}\sqrt{\dfrac{\rho_2}{\rho_1}} - 1}{\dfrac{R_2}{R_1} - \dfrac{R_1}{R_2}} \right) \tag{11}$$

Re-arranging and canceling terms:

$$K = -\frac{\pi V_1}{R_2} \left(\frac{\frac{V_2}{V_1} \frac{R_2}{R_1} \sqrt{\frac{\rho_2}{\rho_1}} - 1}{\frac{R_2}{R_1} - \frac{R_1}{R_2}} \right) \qquad (12)$$

Multiplying R_2 in the denominator and re-arrange to get:

$$K = -\frac{\pi V_1}{R_1} \left(\frac{\frac{V_2 R_2}{V_1 R_1} \sqrt{\frac{\rho_2}{\rho_1}} - 1}{\frac{R_2^2}{R_1^2} - 1} \right) \qquad (13)$$

Equation (13) is the formula used for the stretch rate whenever stretch was solved in this study.

$$R_s = R_2 \cdot \sqrt{1 - \frac{\frac{R_2}{R_1} - \frac{R_1}{R_2}}{\frac{R_2}{R_1} - \frac{V_1}{V_2} \sqrt{\frac{\rho_1}{\rho_2}}}} \qquad (14)$$

Equation (14) is the formula for the stagnation radius. It was solved explicitly by Wang et al. (2006) and that is the formula used throughout this study.

The stretch rate and stagnation radius are dependent on the nozzle radius, R_i, gas density, ρ_i, and velocity, V_i, where the subscript 'i' is 1 for the inner nozzle or fuel and 2 for the outer nozzle or oxidizer as can be seen in Figure 1. It needs to be stated that V_2 is a negative value when solving these equations because the oxidizer flows radially inward (i.e. the negative radial direction). Also, when performing these calculations the temperature and pressure used was 296 Kelvin and 750 Torr respectively. For the opposed tubular flame, the stretch rate at the stagnation surface represents the stretch rate of the flame and the stagnation radius represents the flame radius (the inverse of the stagnation radius represents the curvature on the flame). The stretch rate peaks at the

stagnation surface and as the initial mixture strength is decreased the flame moves closer to the stagnation surface. When the flames are close to the stagnation surface (heavily diluted flames), using the definitions for the stretch rate and stagnation radius of Equations (13) and (14) are appropriate. In CHAPTER IV, the difference between the stagnation radius and flame radius is further discussed as well as the mixture fraction.

It was shown experimentally by Hu et al. (2007) that hydrogen flames have the ability to form cellular structures at high stretch rates and even change orientation from concave to convex curvature. In this thesis, it will be shown that the cellular flame is able to resist curvature altogether and become completely flat facing the incoming flow. It was shown experimentally and numerically by Hu et al. (2007) and Wang et al. (2007) that concave curvature towards the fuel weakens preferential diffusion and convex curvature towards the fuel strengthens preferential diffusion for diluted hydrogen flames with fuel Lewis numbers less than one. The strengthening effect of convex curvature promotes combustion, enhances the flame temperature, and retards extinction to lower initial mixture strengthens and higher stretch rates. It will be shown that cellular flames also have extended flammability limits because of the convex curvature at the flame edges. The strengthening or weakening of the preferential diffusion is related to the ratio of the flame thickness to flame radius. As the flame radius gets smaller, the ratio of the flame thickness to flame radius gets larger and the effect of curvature on preferential diffusion is increased.

V_2, R_2, ρ_2

V_1, R_1, ρ_1

Z

stagnation surface

R
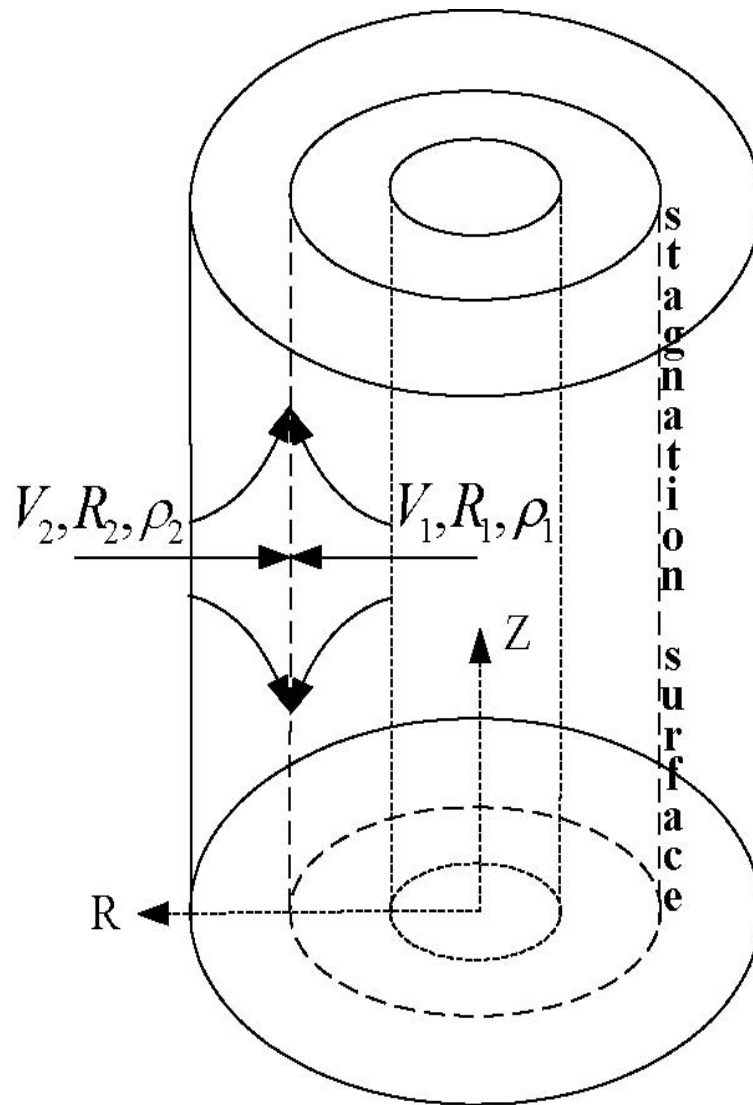
Figure 1: Non-premixed opposed-flow tubular flame flow field

Tubular Flames

There have been lots of studies on flame stretch and non-unity Lewis number flames, but not a lot on flame curvature. Ishizuka (1993) wrote a very thorough analysis on flame curvature but the focus was primarily on premixed flames, with very little pertaining to non-premixed combustion.

Therefore, the NPOF tubular burner is unique because it enables experiments on both stretched and curved diffusion flames. The flames are stretched similar to a planar counterflow burner, but the shape of the flame is tubular with a symmetric cross-sectional shape. The advantage of the tubular shape over planar is that curvature can be studied. The tubular burner has constant curvature, over the flame sheet, which is easy to quantify. The symmetric shape of the tubular flame is a very attractive feature of this burner, and the effects of flame curvature on preferential diffusion cannot be overstated. Comparisons between tubular flames and planar flames are generally used to understand how curvature affects the properties of stretched flames and these comparisons must be based on the same stretch rate. Throughout this study, there will be continuous comparisons between planar and curved flames. Therefore, it was important for Wang et al. (2006) to accurately calculate the stretch rate for the NPOF tubular flame.

An important feature of this burner is that the curvature and stretch can be varied independently. This is possible because their directions are orthogonal to each other. The stretch rate is a manifestation of the flame being pulled in the axial direction and curvature is a manifestation of the flame's location in the radial direction. Both parameters can be solved analytically and the flow field is simple which makes numerical simulations less time consuming (Hu et al., 2007; Wang et al., 2006; Wang et al., 2007).

This is true, even if it is not currently feasible to numerically simulate the complicated three-dimensional cellular structures in the NPOF tubular burner (this is discussed later).

The NPOF tubular burner can be realized by inserting a small tubular porous nozzle along the central axis of the burner. The NPOF tubular flames investigated are positively stretched and negatively curved on the fuel side of the reaction zone. Positive curvature is defined as flame curvature convex to the inner fuel nozzle. Negative curvature is defined as flame curvature concave to the inner fuel nozzle. Positive curvature strengthens preferential diffusion and negative curvature weakens preferential diffusion when the Lewis number of the fuel is less than unity.

CHAPTER III

EXPERIMENTAL SYSTEM

Non-Premixed Opposed-Flow Tubular Burner

Experiments were conducted in the same tubular burner as in a previous premixed experiment (Wang et al., 2009). The only difference between that burner setup and the current one is that a porous inner nozzle is installed along the axis of symmetry to allow non-premixed tubular flames to be produced. The burner can be seen in Figure 2. Besides qualitative study of premixed and non-premixed flames, this multipurpose burner allows for quantitative study of flame parameters because of the three optical ports along the periphery that allow access for laser-based diagnostics.

The new inner fuel nozzle is made of a porous material (Mott Corporation, 5 μm pore size) and is 8 mm in height and 6.35 mm in diameter. The fuel is introduced flowing radially outward from the inner nozzle and the oxidizer is introduced flowing radially inward from the outer nozzle. The contoured outer nozzle of the burner is also 8 mm in height but has a diameter of 24 mm. Figure 1 shows how the two flows meet at a stagnation surface.

The cellular flames form at high stretch rates, near extinction where the effect of buoyancy is negligible[2]. Also, the 8 mm height of the inner and outer nozzles allows for very high stretch rates to be studied before the onset of turbulence.

---

[2] In this study, for flame thicknesses of 2 mm or less the diffusion time is much shorter than the buoyancy time leading to a negligible effect of buoyancy.
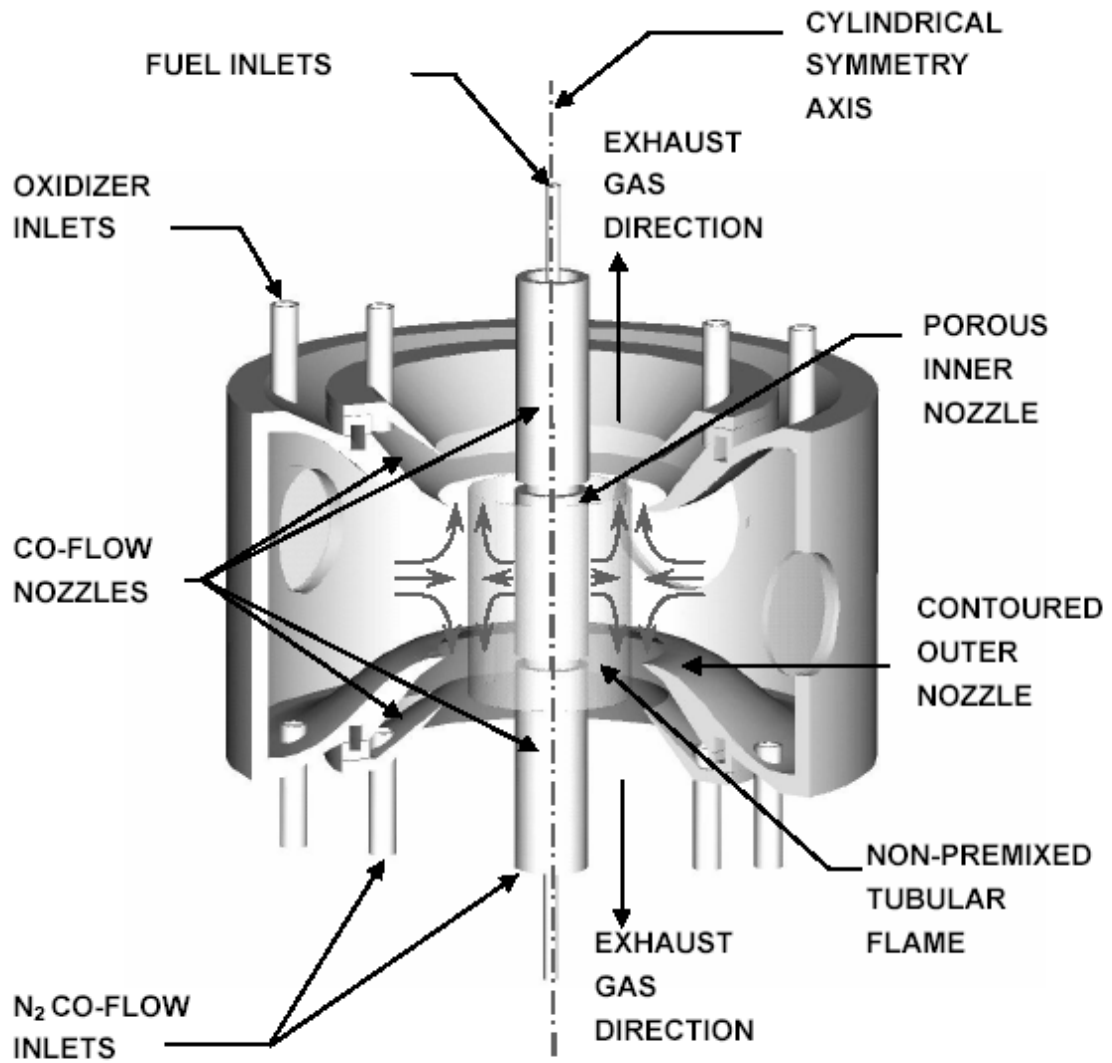
Figure 2: Non-premixed opposed-flow burner

A mirror with a slot-cutout (the slot-cutout was made so the mirror could be positioned around the inner nozzle) is mounted underneath the tubular burner at 45 degrees to the axis of symmetry. This is a very similar optical setup to earlier experiments (Hu et al., 2009a; Wang et al., 2009). The mirror provides a view of the flame as seen from overhead. An ICCD camera (PI-Max 2 fitted with a UV-Nikkor 105 mm f/4.5 lens with high resolution 1024 x 1024 and slow read) is mounted horizontally and records the chemiluminescence emission from the flame reflected off the mirror with the slot-cutout. Figure 3 shows a typical non-cellular tubular flame with the inner nozzle superimposed in the figure to show why the backside of the flame is partially obscured. Even with the inner nozzle partially obscuring the flame image, the high resolution ICCD camera records a much more detailed image of the flame compared to the previous low resolution video ICCD camera (Hu et al., 2009a; Wang et al., 2009). Figure 4 shows a side view from one of the optical access ports displaying the three-dimensional nature of the cellular flames. The bright blue area in the center of the image is a cellular flame (the inner fuel nozzle is not seen). The image (from left to right) shows the side view of one cellular flame, area of local extinction, second cellular flame, area of local extinction, and side view of another cellular flame. The two outer cellular flames appear to have higher burning intensities because from this angle those flamelets are several millimeters thick and the middle cellular flame is roughly ~1 mm thick. Figure 4 is not as clear as Figure 3; therefore top view images will be preferred in this paper.

Experimentally it is difficult to study these flames. It has been shown by Lo Jacono et al. (2003) and Hu and Pitz (2009) that these flames are hard to capture on film because of their blue color and very low luminosity. Hu et al. (2007) and Hu and Pitz

(2009) displayed the numerous difficulties in conducting laser diagnostic experiments with this burner: in the fuel rich area of the burner close to the inner fuel nozzle C_2 LIF interferes with the N_2 signal, scattered laser light from the optical access windows and inner fuel nozzle interferes with the signal, and the 3-D nature of the cellular flames makes the application of the 1-D laser diagnostic more difficult and laborious. As a result, Raman measurements have only been conducted in noncellular and completely symmetric concave flames and physical probes affect the flow in the vicinity of the cellular instabilities too much for accurate measurements. This ICCD camera has the capability to record a numeric value for the chemiluminescence that can quantify the burning intensity at any spectral location as well as zooming into regions of greater interest for more thorough investigation. With the ability to quantify the burning intensity, it is possible to observe the flame locations of highest reactivity.
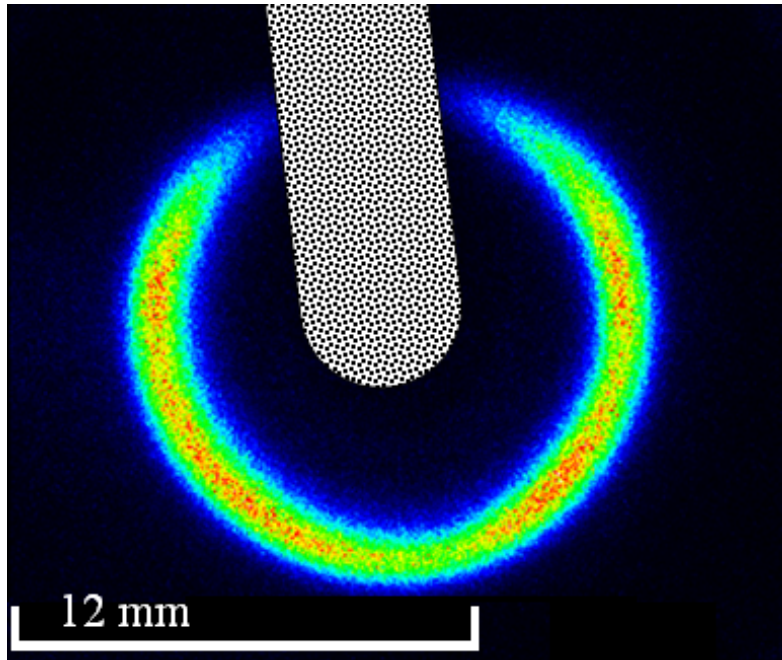
Figure 3: Noncellular flame image obscured by the inner fuel nozzle for 21.7% H_2 diluted in CO_2 versus air opposed tubular flame
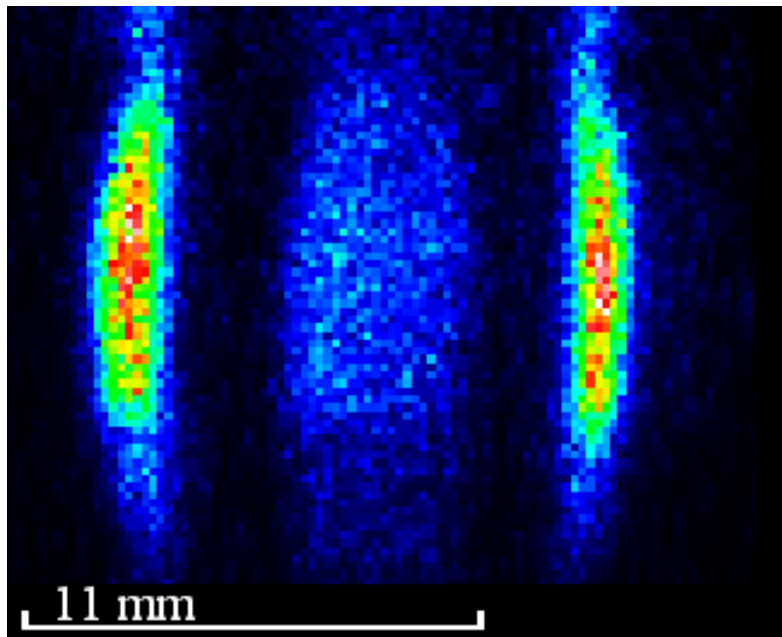
Figure 4: Side view displaying the three-dimensional nature of these cellular flames for $\Phi=0.455$ and K= 88 1/s. Inner fuel nozzle is not shown. From left to right: side view of one cellular flame, area of local extinction, second cellular flame, area of local extinction, and side view of another cellular flame. The two outer cellular flames appear to have higher burning intensities because from this angle those flames are several millimeters thick and the middle cellular flame is roughly ~1 mm thick.

<center>Procedure</center>

The gas flows are controlled by mass flow controllers (Teledyne Hastings HFC-202 and HFC-203) through a computer. The mass flow controllers have an accuracy and linearity of ±1% full scale. The fuel used in this experiment was H_2 diluted with CO_2 and the oxidizer was always air. All gas flows are introduced at room temperature and pressure. The burner is also equipped with a water cooling line which was run throughout the duration of the experiments and a N_2 co-flow which shields the flame from outside perturbations.

As can be seen in Table 1, three different procedures were employed. All tests flows are given in Table 1 unless explicitly stated otherwise in their respective sections in CHAPTER IV Results. Procedure 1: the flame was ignited at a condition where a noncellular flame was seen and far from any instability regime. Then the H_2 flowrate was decreased in steps of 0.5% of the full scale [full scale is 1 standard liter per minute (slpm)] of the mass flow meter until extinction was realized. The CO_2 and air flowrates were kept constant throughout the course of the tests. Three different air velocities of air were used for Procedure 1: 30.4 cm/s, 60.7 cm/s, and 91.1 cm/s. The three different velocities test three different levels of stretch and curvature. As the oxidizer velocity was increased so was the stretch rate and curvature of the flame. Procedure 2: the flame was ignited at a condition where a noncellular flame was seen and far from any instability regime. Then the CO_2 flowrate was increased in steps of 0.333% of the full scale [full scale is 3 standard liter per minute (slpm)] of the mass flow meter until extinction was realized. The H_2 and air flowrates were kept constant throughout the course of the tests. The same three oxidizer velocities were used as in Procedure 1. Procedure 3: the flame

<center>27</center>

was ignited at a condition where a noncellular flame was seen and far from any instability regime. Then the air flowrate was increased in steps of 1% of the full scale [full scale is 100 standard liter per minute (slpm)] of the mass flow meter until extinction was realized. The H_2 and CO_2 flowrates were kept constant throughout the course of the tests. The full scale step size changes for each test were carefully chosen because of their high repeatability of onset of cellularity and extinction conditions and to minimize the effects of momentum perturbations to the already unstable flame. It is important to note that regardless of using Procedure 1, 2, or 3, the flame responds the same whether increasing the stretch rate or decreasing the initial mixture strength because both are reducing the Damköhler number (i.e. moving towards extinction).

The first cellular state was chosen as the first time that there existed at least two separated cells. This was chosen to be the onset of cellularity and not when the noncellular flame initially broke at one location. The condition when two separated cells existed at the same time was a much more consistent flow condition and offered a much higher repeatability of results than when the flame broke at just one location.

The procedure of progressing from a noncellular flame towards extinction is called the positive process. The same procedures were employed but oppositely in the negative process (progressing from very near extinction towards re-establishing a noncellular flame). The goal of the negative process was to evaluate the flame hysteresis and to see if a noncellular flame could be re-established. Lastly, the positive process was conducted again and this time mechanical perturbations were employed. The flame was perturbed with different sizes of wires and metal rods to try to induce cellularity at an earlier condition, obtain multiple cellular states at the same condition, and cause

extinction at an earlier condition. Experiments with mechanical perturbations to cellular flames have been conducted by other researchers (Lo Jacono et al., 2003; Lo Jacono and Monkewitz, 2007) in axisymmetric but not in tubular opposed-flow burners.

Table 1: Flow conditions of the positive process

	Φ (Initial Mixture Strength)*	Air Flowrate (slpm)*	H_2 Flowrate (slpm)*	CO_2 Flowrate (slpm)*	Total Fuel Velocity (cm/s)*	Air Velocity (cm/s)*	K (1/s)*	R_s (mm)*
Procedure 1	.469-.356	10	.265-.190	1.08	15.6-14.7	30.4	89-86	5.3-5.2
	.483-.402	20	.275-.220	1.08	15.7-15.0	60.7	166-163	4.4
	.504-.433	30	.290-.240	1.08	15.8-15.3	91.1	245-240	4.1
Procedure 2	.470-.298	10	0.3	1.22-2.1	17.6-27.8	30.4	90-95	5.4-6.3
	.500-.366	20	0.3	1.13-1.65	16.5-22.6	60.7	168-167	4.5-4.9
	.518-.420	30	0.3	1.08-1.4	16.0-19.7	91.1	246-243	4.1-4.3
Procedure 3	0.518	32-53	0.3	1.08	16.0	97.2-160.9	261-425	4.0-3.7

*First value is onset of cellularity and second value is extinction condition unless there is only one value and that means that the conditions did not change throughout the course of the tests

CHAPTER IV

RESULTS

Numerical Simulations

In Figure 5, the extinction stretch rate of a tubular flame using a 1D simulation is compared to the experimental results of the onset of cellularity for the same flame (it should be noted that this graph is numerical extinction stretch rate versus experimental onset of cellularity, not experimental extinction). Five tests were performed and each flame was 21.7% H_2 diluted with CO_2 versus air. Table 2 provides the composition data for the test flows. The test conditions were chosen to provide constant $Le_{fuel} = 0.35$ and Φ $= 0.518$. This was chosen in order to assess the accuracy of the 1D numerical simulations versus the experimental results solely on a basis of stretch and curvature. The flame is ignited at a condition where a noncellular flame was seen and far from any instability regime. Then the oxidizer flowrate was increased in steps of 1% of the full scale of the mass flow meter until extinction was realized. The fuel was kept constant throughout the course of the tests. It should be noted, that the oxidizer flowrate, oxidizer velocity, stretch rate, and stagnation radius given in Table 2 were that of the onset of cellularity and not the initial condition of the test. The information provided in Table 2 for the fuel did not change throughout the course of the experiments. Therefore the initial composition of the fuel and the end composition were the same.

The numerical code has been described in Wang et al. (2007) and validated in Hu et al. (2007). To represent the current experimental conditions more accurately, the

31

following changes have been made: i) the fixed species mass fraction has been changed to a fixed species flux (Wang et al., 2006) since the species gradients exist at the inner nozzle boundary; ii) although the temperature gradient at the inner nozzle is small for our test cases, the fixed temperature boundary condition has been changed to $\lambda \cdot \left.\dfrac{dT}{dR}\right|_{R_1} = \rho_1 V_1 c_p (T_{R_1} - T_1)$ for best accuracy (heat transfer to the nozzle heats the fuel stream); and iii) the optical thin radiation model has been added for CO_2 and H_2O.

As seen in Figure 5, the onset of cellularity appears experimentally very near the 1D numerical extinction limit at low fuel velocities and above the 1D numerical extinction limit at high fuel velocities. This is a graph of numerical extinction versus onset of cellularity; these flames exist experimentally until a much higher stretch rate. The extinction of these flames is not recorded here because at high stretch rates, near extinction, the flame is very close to the inner fuel nozzle and heat loss to the burner can be great. All the data shown in Figure 5 are for conditions where the flame is far from the fuel nozzle and there is negligible heat loss to the burner surface. The existence of a cellular flame outside the flammability limit predicted by 1D numerical simulation is consistent with earlier results (Lee and Kim, 2002).

The 1D numerical code that was described by Wang et al. (2007) and validated by Hu et al. (2007) is unable to accurately predict the extinction of flames whose Lewis number is far from unity. This is because of the existence of multi-dimensional cellular structures. An explanation of this sublimit phenomenon is given in CHAPTER V Discussion Section.
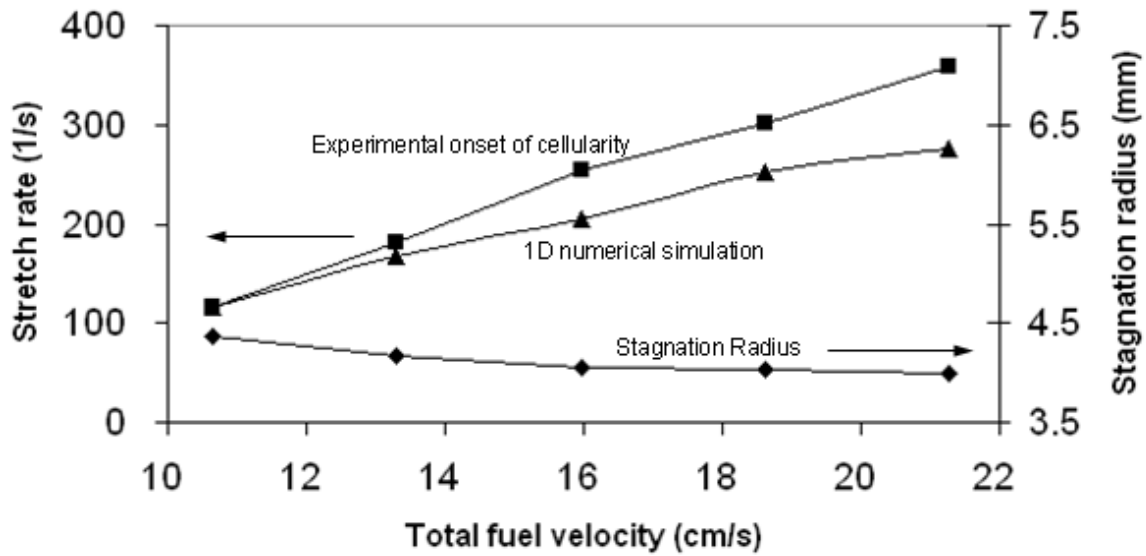
Figure 5: 1D numerical simulation of extinction versus experimental onset of cellularity in 21.7% H_2 diluted in CO_2 versus air opposed tubular flames

Table 2: Composition of flows for numerical code versus onset of cellularity study for 21.7% H_2 diluted in CO_2 versus air opposed tubular flames

Test Number	Oxidizer flowrate (slpm)*	Hydrogen flowrate (slpm)	Carbon dioxide flowrate (slpm)	Velocity of fuel (cm/s)	Velocity of oxidizer (cm/s)*	Stretch Rate (1/s)*	Stagnation Radius (mm)*
1	14.0	0.200	0.720	10.64	42.50	117.0	4.4
2	22.0	0.250	0.900	13.30	66.79	181.4	4.2
3	31.0	0.300	1.080	15.96	94.11	253.5	4.0
4	37.0	0.350	1.260	18.62	112.33	302.2	4.0
5	44.0	0.400	1.440	21.28	133.58	358.8	4.0

*experimental oxidizer flowrate, oxidizer velocity, stretch rate, and stagnation radius at onset of cellularity

Onset of Cellularity

Figure 6 displays the process of a noncellular flame progressing to six edge flames. Table 3 provides the composition data for each individual image. The flame was ignited at a noncellular condition that was far from any instability regime. Then the oxidizer flowrate was increased in steps of 1% of the full scale of the mass flow meter, while the fuel was kept constant throughout the course of the tests. The labels of the figure number and letter on the left most column of Table 3 provide the experimental conditions of the images seen in Figure 6. In Figure 6, the Lewis number and initial mixture strength are kept constant but the stretch rate is increasing and the stagnation radius is decreasing (the stretch rate increases by over 37.5% while the stagnation radius only decreases by 8.5%, so the effect of stretch is dominant). The images in Figure 6 were chosen to be the best display of a noncellular flame progressing to six edge flames. A noncellular flame is shown in Figure 6 (a), the noncellular flame initially broke at one location in Figure 6 (b), the onset of cellularity occurs in Figure 6 (c), and the progression of more cells forming is shown in Figures 6 (d) through (i).

Figure 7 displays a graph showing how the stretch rate increases and the stagnation radius decreases as the oxidizer velocity is increased. The oxidizer is introduced from the outer nozzle and flows radially inward. As the flowrate of the oxidizer is increased, the stretch rate increases and flame is pushed closer to the inner fuel nozzle. The progress from six edge flames to extinction is not shown because the heat loss to the inner nozzle is going to be significant for those cases. Figure 6 clearly shows the strength of the flame edges. The flame edges are locally convex to the fuel stream (positive curvature) although the overall tubular flame is concave to the fuel stream. Even

at high stretch rates, the convex edge flames are clearly stronger than the concave curved flames. This is shown by the convex edge flames displaying a higher burning intensity and a larger flame thickness. The strong strengthening effect of positive curvature on the preferential diffusion applies to cellular flames alike, as the locations of local positive curvature are the strongest areas of the flame.

These flames display a strong chemiluminescence emission coming from the edge locations. Even at a much lower stretch rate as in Figure 6 (b), the chemiluminescence emission coming from the edge flames is much stronger than anywhere else on the concave curved flame. The preference of convex curvature for tubular diffusion flames when the Lewis number is less than unity is also shown in the breaking of one cell to become two cells [as seen in Figure 6 (e) to (f)]. Additional experiments were conducted using the same Lewis number, initial mixture strength, and fuel composition by more slowly increasing the stretch rate in order to elucidate the process of cells splitting to form new cells.

Figure 8 shows a zoomed-in progression of one cell becoming two cells. This is just one example but it provides a general experimental display of cell formation. In Figure 8, the Lewis number, initial mixture strength, and stagnation radius are kept constant and the stretch rate is increased by increasing the oxidizer flowrate (the stagnation radius is actually decreasing slightly 2.5% while the stretch rate increased 12.5%; therefore the increase in the stretch is much more dominant than the increase in overall flame curvature). Also to better assess the effect of stretch, the oxidizer flowrate was increased in steps of 0.5% of full scale instead of 1%. In Figure 8, as the stretch rate is increased it is possible to see the flame midsection thin and eventually break. Also as

stretch is increased, the strong burning locations on both sides of the midsection become almost flat to the incoming fuel flow. The concave curvature at the midsection eventually leads to local flame extinction. Throughout the whole process, the edge flames don't thin and are almost unaffected by increasing stretch because of their convex curvature.
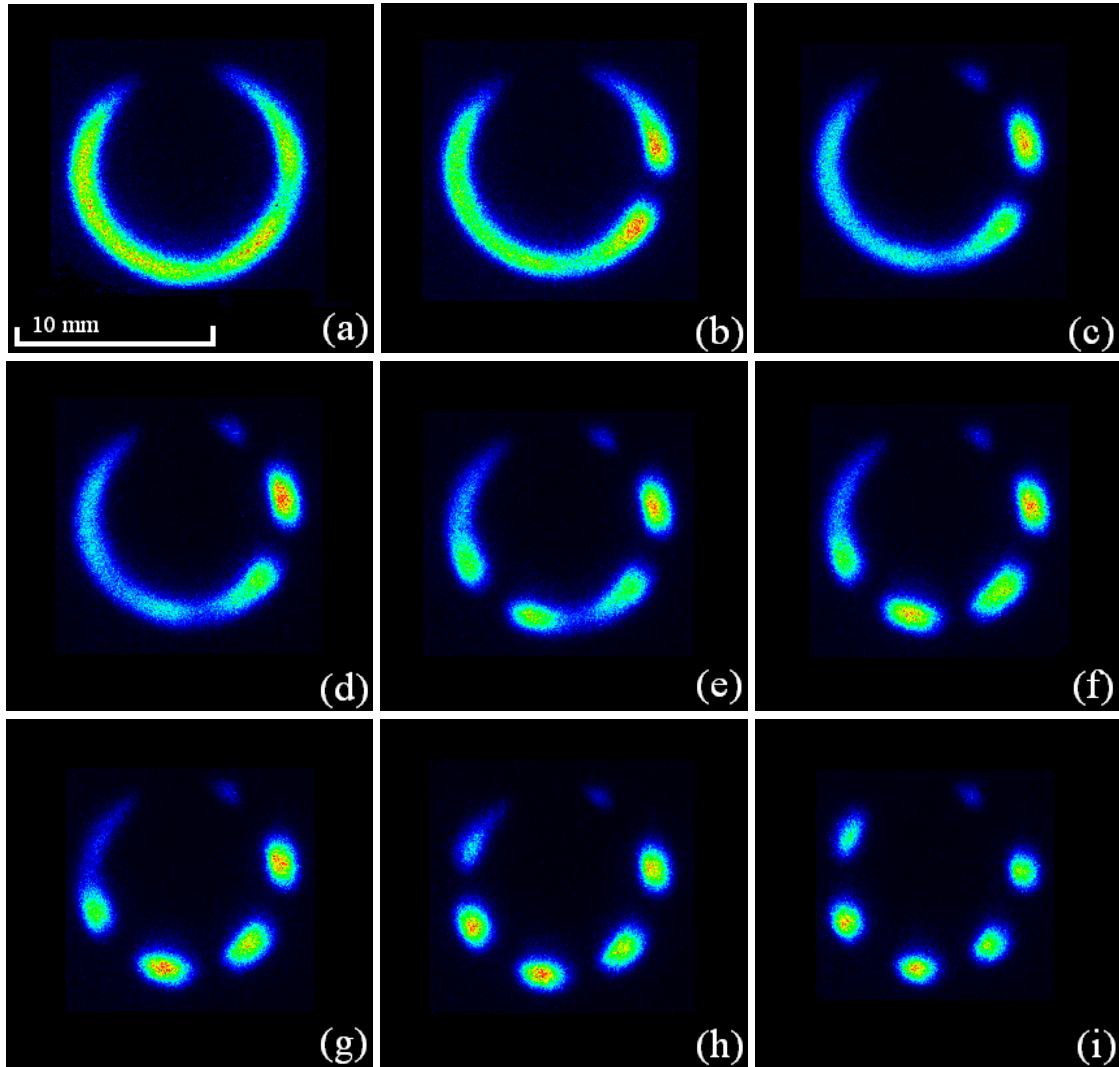
Figure 6: Progression of cell formation with increasing oxidizer flowrate in 21.7% H2 diluted in CO_2 versus air opposed tubular flames with $\Phi = 0.518$ and $Le_{fuel} = 0.35$. (a) K= 207 1/s, (b) K= 238 1/s, (c) K= 261 1/s, (d) K= 277 1/s, (e) K= 285 1/s, (f) K= 292 1/s, (g) K= 324 1/s, (h) K= 331 1/s, (i) K= 386 1/s

Table 3: Experimental data for the cell formation process with increasing oxidizer flowrate for 21.7% H_2 diluted in CO_2 versus air opposed tubular flames

Figure	Oxidizer flowrate (slpm)	Hydrogen flowrate (slpm)	Carbon dioxide flowrate (slpm)	Velocity of Fuel (cm/s)	Velocity of Oxidizer (cm/s)	Stretch Rate (1/s)	Stagnation Radius (mm)	Cellularity and number of cells
6 (a)	25	0.30	1.08	16	76	207	4.2	Noncellular
6 (b)	29	0.30	1.08	16	88	238	4.1	Broken cell
6 (c)	32	0.30	1.08	16	97	261	4.0	2 Cells*
6 (d)	34	0.30	1.08	16	103	277	4.0	3 Cells**
6 (e)	35	0.30	1.08	16	106	285	4.0	4 Cells**
6 (f)	36	0.30	1.08	16	109	293	3.9	5 Cells**
6 (g)	40	0.30	1.08	16	121	324	3.9	5 Cells**
6 (h)	41	0.30	1.08	16	124	331	3.9	6 Cells**
6 (i)	48	0.30	1.08	16	146	386	3.8	6 Cells**

  *   onset of cellularity
** one cell is partially obscured by the inner fuel nozzle
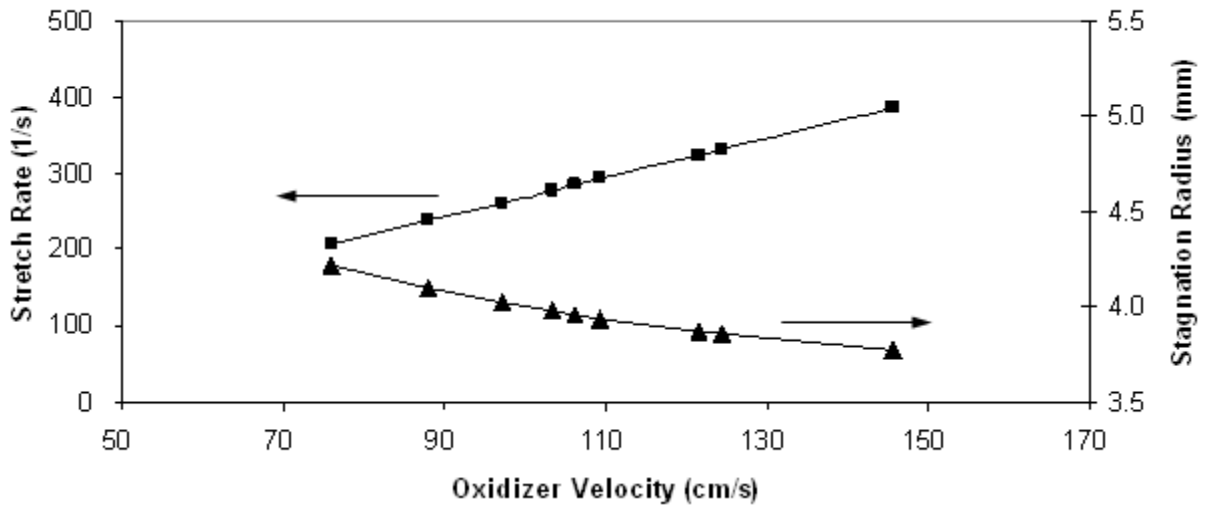
Figure 7: Dependence of calculated stretch rate and stagnation radius on increasing oxidizer flowrate in 21.7% H_2 diluted CO_2 versus air opposed tubular flames
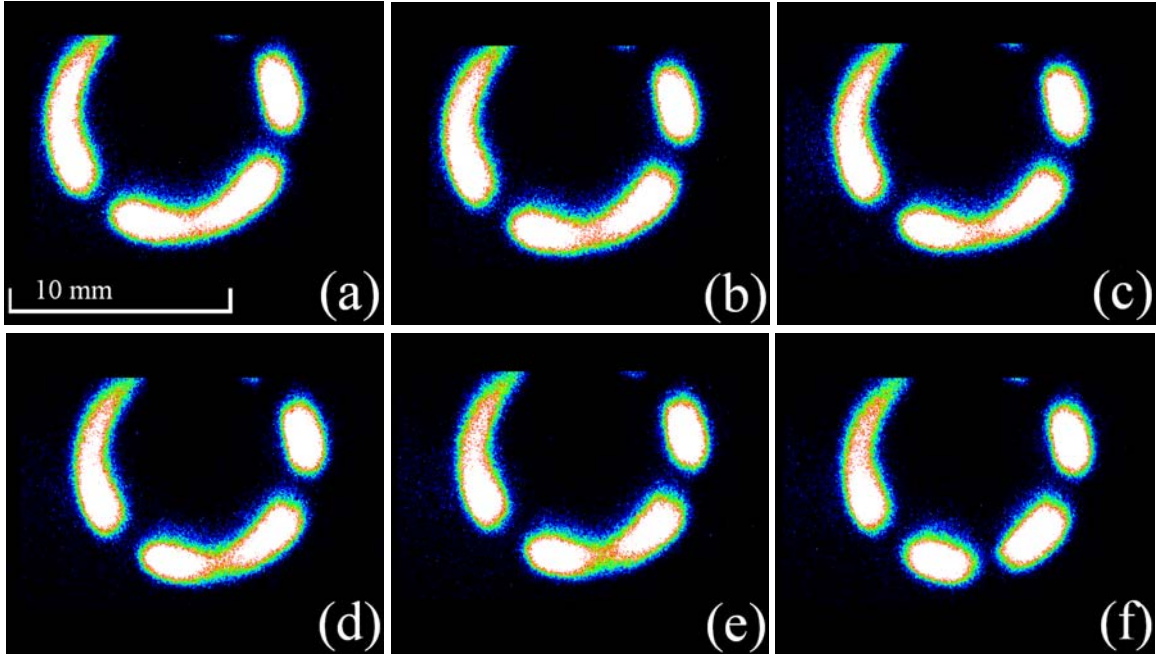
Figure 8: Progression of cell formation with increasing the stretch rate showing strong flame edges and thinning inside of cells for 21.7% H_2 diluted in CO_2 versus air opposed tubular flames with Φ = 0.518 and Le_{fuel} = 0.35. (a) K=246 1/s, (b) K=254 1/s, (c) K=261 1/s, (d) K= 269 1/s, (e) K= 277 1/s, (f) K= 281 1/s

A. Positive Process Procedure 1

Using Procedure 1, the flame could be judged solely on the basis of lowering the initial mixture strength. As can be seen in Table 1, the stretch rate and stagnation radius are almost constant throughout the course of the tests. Keeping the stretch rate constant, the flame did not experience a larger stretch rate as noncellular than at the extinction condition. Keeping the stagnation radius constant, the curvature of the noncellular and cellular flame did not change and the heat loss to the inner fuel nozzle was no greater when the flame was noncellular than at the extinction condition. Figure 9 shows a graph of the calculated stagnation radius versus the measured flame radius using Procedure 1 with an air velocity of 30.4 cm/s. The flame radius was judged by the peak chemiluminescence from the flame. Figure 9 shows that the flame location did not change significantly throughout the course of the test and that the flame always resides on the oxidizer side of the stagnation radius. As can be seen in Figure 9, as the flame becomes more diluted (i.e. lower initial mixture strength), the flame location moves closer to the stagnation surface. This agrees well with other results of diluted H_2 versus air flames in a planar counterflow burner (Brown et al., 1997).

Figure 10 shows the progress of a flame from noncellular to near extinction using Procedure 1 with an air velocity of 30.4 cm/s. As can be seen in Figure 10, the flame thickness is almost constant; but the flame length (distance between the highly curved flame edges) is seen to decrease substantially. It was also seen that while the flame was in the process of breaking up into cells [Figure 10 (b)], the flame edges displayed a much greater flame thickness and burning intensity than the concave flame. This is seen in

Figure 10 but not as significantly as in Figure 14 (Procedure 3), this will be discussed later. Once the maximum number of cells is achieved, the cellular flames are almost flat facing the opposing flows with highly curved flame edges. The flames very near extinction are highly curved and are almost perfectly circular.

Figure 9: Measured flame radius (■) based on peak chemiluminescence and calculated stagnation radius (♦) versus initial mixture strength for opposed tubular flames using Procedure 1 positive process with air velocity at 30.4 cm/s and K= ~86 1/s

Figure 10: Progression of cell formation with decreasing initial mixture strength for opposed tubular flames using Procedure 1 positive process with air velocity at 30.4 cm/s, K= ~86 1/s, and R_s= ~5.2 mm. One cell is blocked by the inner fuel nozzle. (a) Φ=0.518, (b) Φ=0.469, (c) Φ=0.462, (d) Φ=0.433, (e) Φ=0.411, (f) Φ =0.388, (g) Φ =0.364

B. Positive Process Procedure 2

As can be seen in Table 1, the stretch rate and stagnation radius are almost constant throughout the course of the tests using Procedure 2 and at the same oxidizer velocity the stretch rate and stagnation radius of Procedure 2 are very close to that of Procedure 1. In actuality, the stagnation radius is not constant but is increasing as the flame progresses towards extinction. Since the CO_2 is introduced from the inner fuel nozzle, increasing the CO_2 flowrate increases the stagnation radius. This means that the curvature of the flame as noncellular was greater than at near extinction conditions. Figure 11 shows a graph of the stagnation radius versus the flame radius using Procedure 2 with an air velocity of 30.4 cm/s. Figure 11 shows that the flame location moved towards the outer nozzle throughout the course of the test and that the flame location is on the oxidizer side of the stagnation radius. When increasing the CO_2 flow, the stagnation radius moves away from the inner fuel nozzle more than the actual flame location. Once again, this agrees well with other results of diluted H_2 versus air flames (Brown et al., 1997).

Figure 12 shows the process of a flame from noncellular to near extinction using Procedure 2 with an air velocity of 30.4 cm/s. Just like in Procedure 1, the flame thickness is almost constant whereas the flame length experiences a great reduction in size. While the noncellular flame is breaking up into cells, it can be seen that the flame experiences gradients in the chemiluminescence[3] as seen in Figures 12 (b) and (c). These gradients are more pronounced than Procedure 1 but still not as significant as Procedure

---

[3] A gradient in chemiluminescence is used to describe the difference in burning intensity from one location to another on the flame. This method of visually describing flames has already been employed by Lo Jacono et al. (2003) and Lo Jacono and Monkewitz (2007), but not with images of this clarity. As can be seen, the flame edges display a much greater burning intensity than the weaker middle sections of the flame. That is what is meant by chemiluminescence gradient.

3. To the authors' knowledge, the chemiluminescence gradient in the flame displaying the splitting of one cell to form two cells has never been seen with such clarity before now. Overall, the flame images of Figure 12 appear relatively similar to those of Figure 10. Very near extinction the cellular flames appear circular.
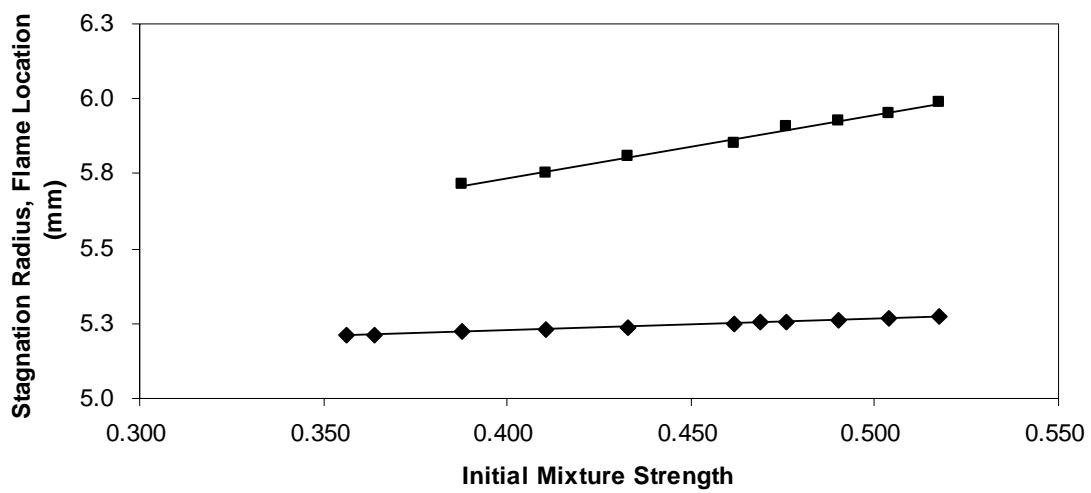
Figure 11: Measured flame radius (■) based on peak chemiluminescence and calculated stagnation radius (♦) versus initial mixture strength for opposed tubular flames using Procedure 2 positive process with air velocity at 30.4 cm/s and K= ~90 1/s
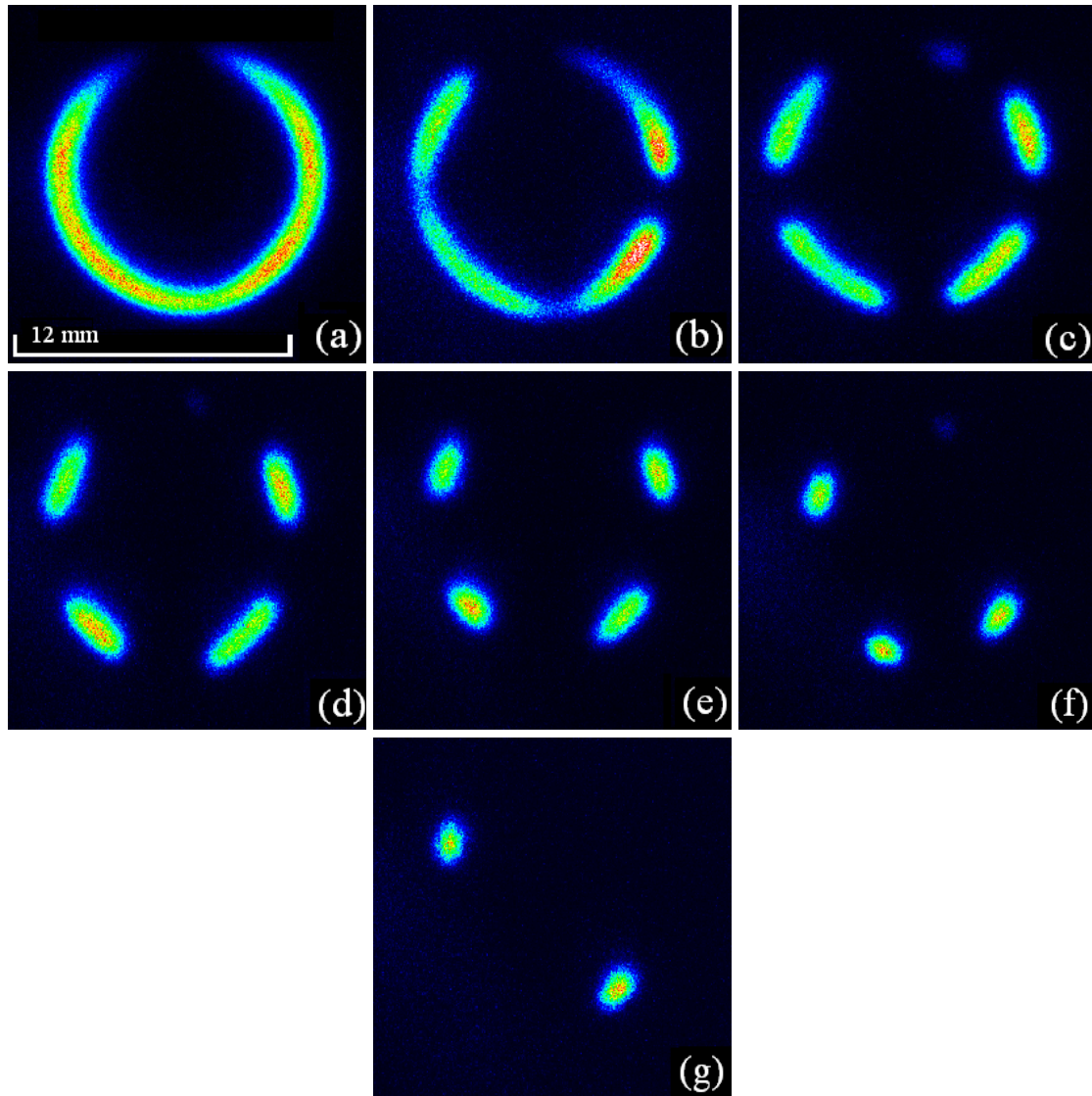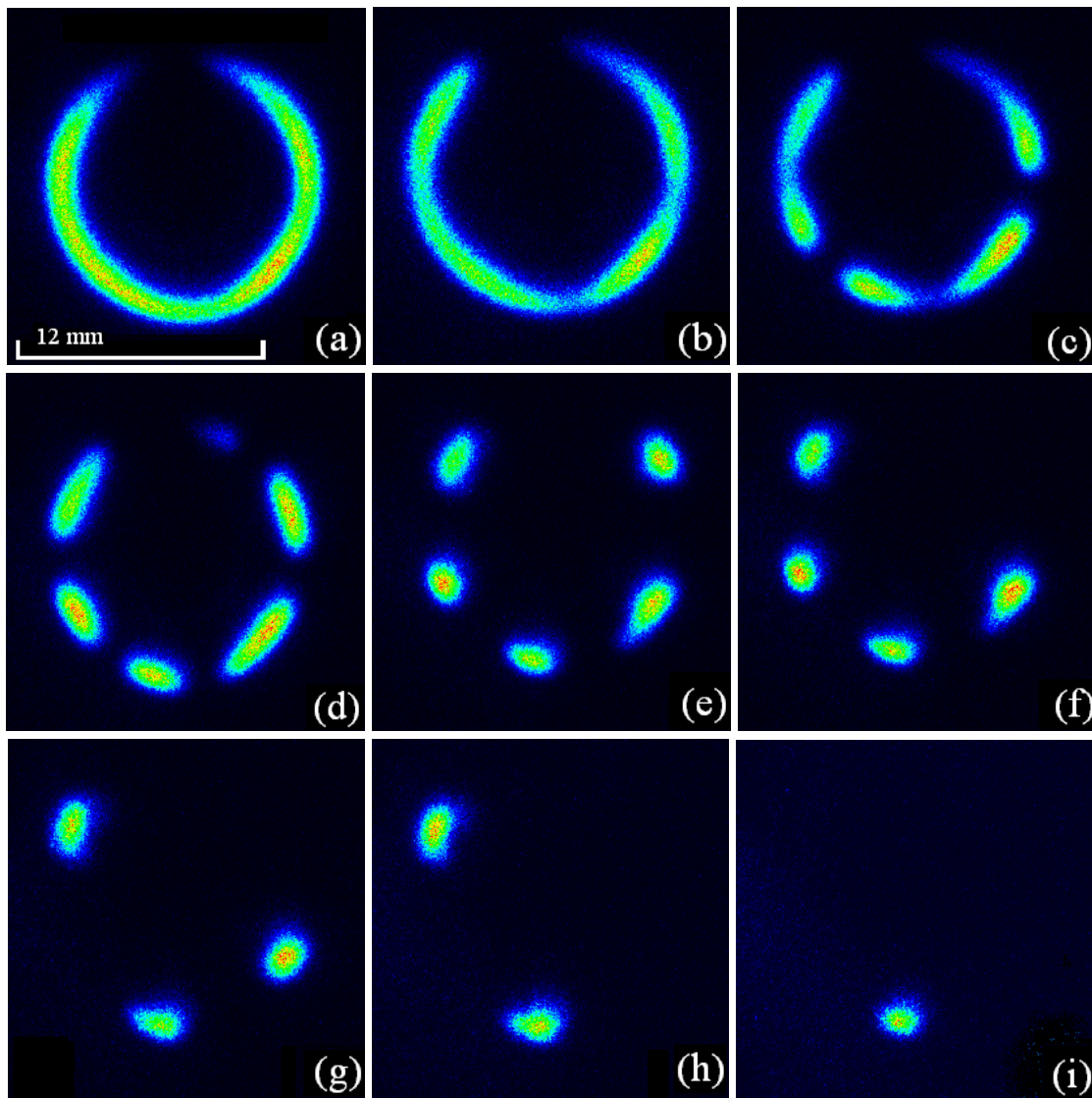
Figure 12: Progression of cell formation with decreasing initial mixture strength in opposed tubular flames using Procedure 2 positive process with air velocity at 30.4 cm/s and K= ~90 1/s. One cell is blocked by the inner fuel nozzle. (a) Φ=0.510, (b) Φ=0.476, (c) Φ=0.470, (d) Φ=0.464, (e) Φ=0.376, (f) Φ=0.359, (g) Φ=0.339, (h) Φ=0.329, (i) Φ=0.312

C. Positive Process Procedure 3

Using Procedure 3, the flame could be judged solely on the basis of increasing the stretch rate and flame curvature while the initial mixture strength and Lewis number were kept constant. As can be seen in Table 1, the stretch rate and stagnation radius are increasing and decreasing, respectively. Flame curvature is the inverse of the stagnation radius; a large stagnation radius means a small curvature. This was the only test that was conducted with a significantly decreasing stagnation radius. Moving the flame closer to the inner fuel nozzle makes it possible to judge the flame response to increased curvature. It is difficult to assess the effects of heat loss to the inner fuel nozzle on flame extinction. This paper does not go into the effects of heat loss on extinction. Instead, the focus is on the effects of increasing stretch and curvature on flame instability far from extinction and comparing the flame images of Procedures 1, 2, and 3.

Figure 13 shows a graph of the stagnation radius versus the flame radius with respect to the stretch rate. Figure 13 shows that the flame location is always on the oxidizer side of the stagnation radius and that the flame location stayed at a constant distance from the stagnation surface throughout the course of the test. The stoichiometric mixture fraction (ξ_{st}) of this 21.7% H_2 diluted in CO_2 versus air flame is $\xi_{st} = 0.7$. This indicates the flame should reside on the fuel side under equal species diffusion. However, the strong non-unity specie diffusivity causes the flame to reside on the oxidizer side; this is consistent with a previous study of a 20% H_2 diluted in N_2 versus air planar flame ($\xi_{st} = 0.62$) where the flame also resided on the oxidizer side (Brown et al., 1997).

Figure 14 shows the flame images of Procedure 3. The flame thickness is fluctuating heavily throughout the process of transitioning from noncellular to cellular.

48

While the flame was in the process of forming cells, the flame edges displayed a much greater thickness and higher burning intensity than the rest of the flame. This is more dramatic than in Procedure 1 or 2. It is easy to see the thinning of certain locations to form two distinct cells from one long cell. One long cell displays more concave curvature than two shorter cells. The effects of curvature on preferential diffusion and flame temperature have been shown numerically (Wang et al., 2007; Hu and Pitz, 2009). To the author's knowledge, this is the first time it has been possible experimentally to display with this clarity burning intensity gradients in cellular flames.

Figure 14 (c) to (e) show that the concave curved flames displayed a significant reduction in flame thickness and burning intensity than the flame edges. The burning intensity drops from its noncellular burning intensity while the flame is breaking up into cells. Once the flame is fully cellular and broken up into multiple cells, the flame's burning intensity increases back to the noncellular level and even higher for a certain range of flow conditions. This is because of the convex curvature of the flame edges. Numerical findings (Hu and Pitz, 2009) show a convex flame can have a flame temperature of 100-200 Kelvin higher than a concave flame at the same flow conditions. The flames very near extinction are almost perfectly circular.
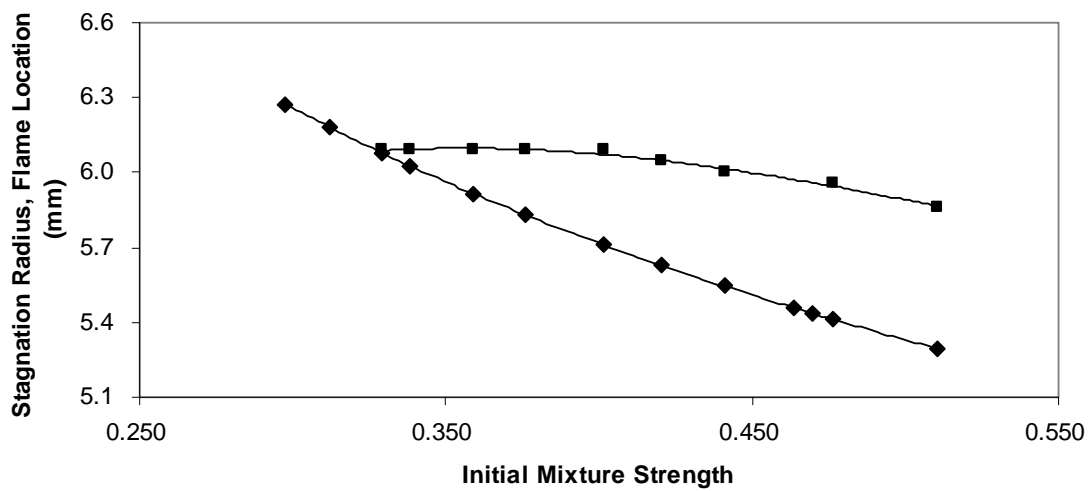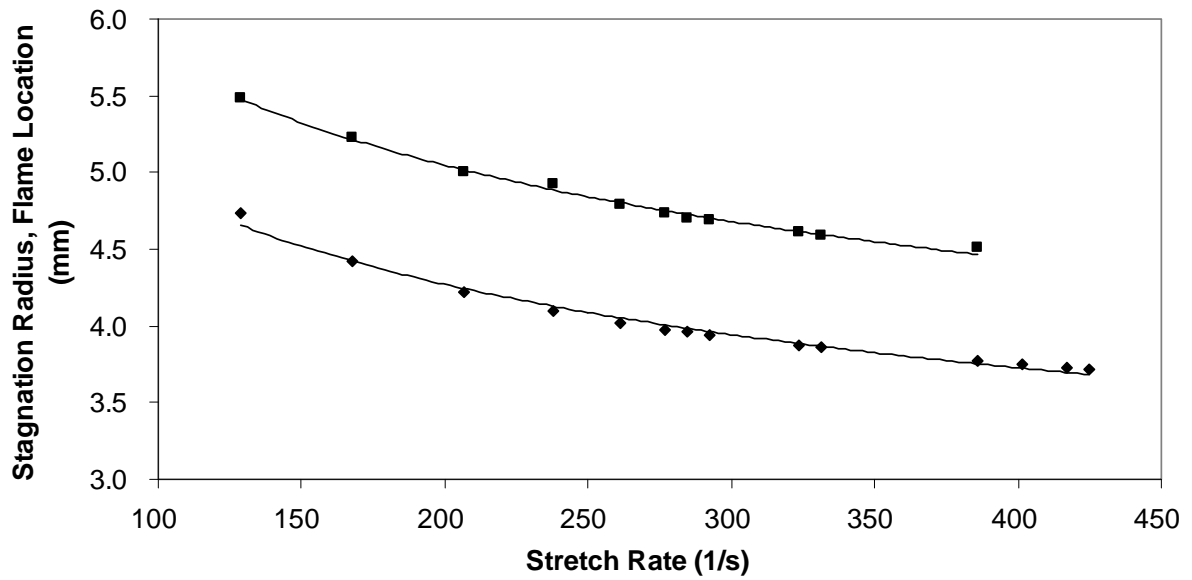
Figure 13: Measured flame radius (■) based on peak chemiluminescence and calculated stagnation radius (♦) versus stretch rate in opposed tubular flames using Procedure 3 for the positive process with $\Phi = 0.518$ and $Le_{fuel} = 0.35$
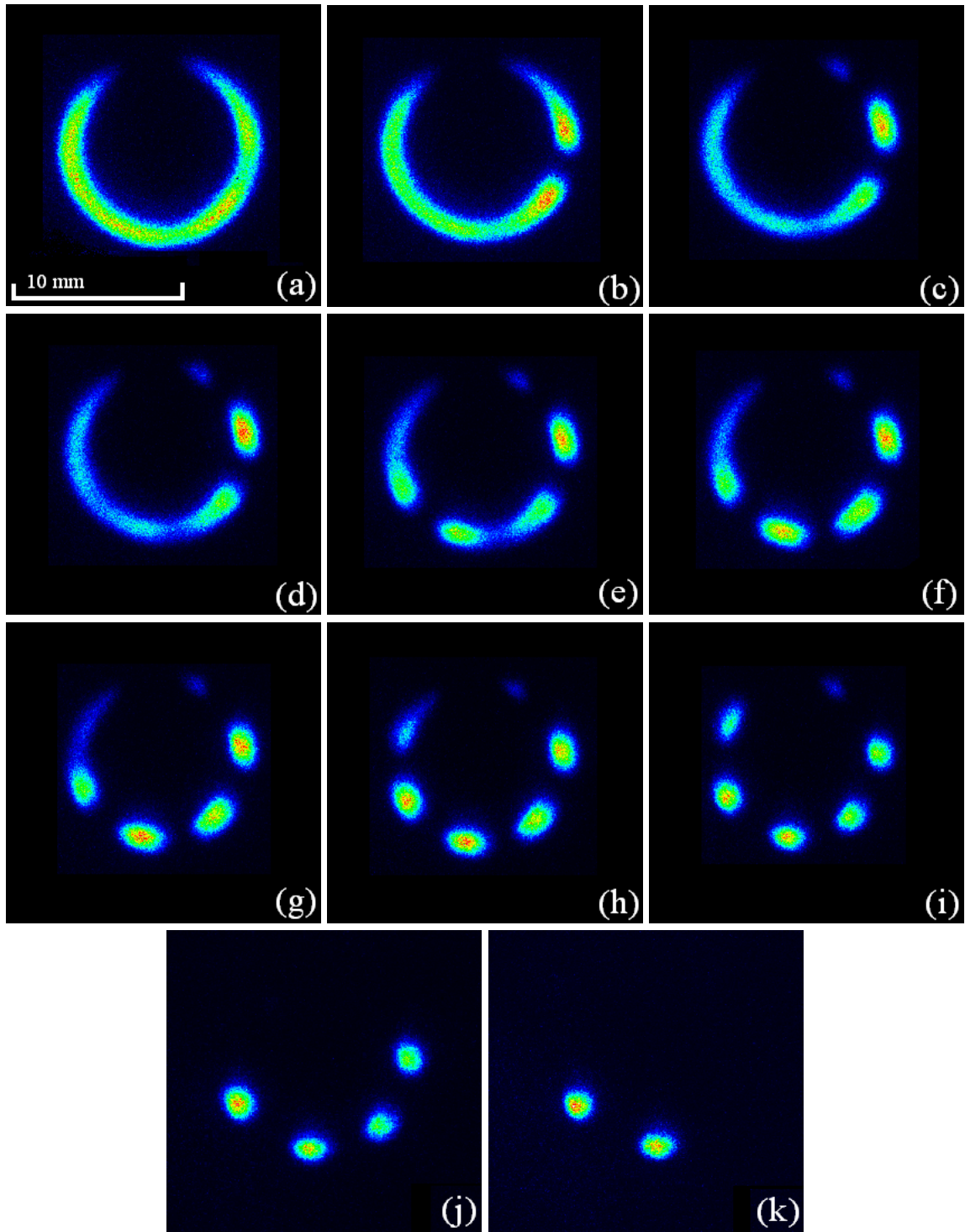
Figure 14: Progression of cell formation with increasing oxidizer flowrate for opposed tubular flames using Procedure 3 positive process with $\Phi = 0.518$ and $Le_{fuel} = 0.35$. One cell is blocked by the inner fuel nozzle. (a) K=207 1/s, (b) K=238 1/s, (c) K=261 1/s, (d) K=277 1/s, (e) K=285 1/s, (f) K=292 1/s, (g) K=324 1/s, (h) K=331 1/s, (i) K=385 1/s, (j) K=402 1/s, (k) K=417 1/s

Table 4 shows the flow conditions for the negative process. The negative process began at a condition near extinction and progressed towards re-establishing a noncellular flame. Procedure 1 was conducted again with the air velocity of 30.4 cm/s and 91.1 cm/s. The test began at a condition very near the extinction limit and then the H_2 flowrate was increased in steps of 0.5% of the full scale of the mass flow meter until the flame became noncellular. The CO_2 and air flowrates were kept constant. As can be seen in Table 4, Procedures 2 and 3 were also conducted. Procedure 2: the CO_2 flowrate was decreased in steps of 0.333% of the full scale of the mass flow meter until the flame became noncellular. The H_2 and air flowrates were kept constant. Procedure 3: the air flowrate was decreased in steps of 1% of the full scale of the mass flow meter until the flame became noncellular. The H_2 and CO_2 flowrates were kept constant. The full scale step size changes and flow conditions were chosen to mimic the positive process as best as possible.

Figure 15 shows a graph comparing the number of cells versus the initial mixture strength for the positive process and the negative process using Procedure 2 with air velocity at 91.1 cm/s. In Figure 15, the point of highest initial mixture strength represents the transition from noncellular to cellular for the positive process (or cellular to noncellular for the negative process), and this occurs in the negative process at a higher value than in the positive process. The lowest initial mixture represents the extinction condition. Figure 16 shows a graph comparing the number of cells versus the stretch rate for the positive process and the negative process using Procedure 3. In Figure 16, the point of lowest stretch rate represents the transition from noncellular to cellular for the

positive process (or cellular to noncellular for the negative process), and this occurs in the negative process at a lower value than in the positive process. The highest stretch rate represents the extinction condition. Comparing Figures 15 and 16, the transition from the onset of cellularity until the point when the maximum number of cells was achieved occurred much faster in Procedure 2 than Procedure 3. This indicates that cell formation is much more sensitive to a decrease in initial mixture strength than increase in stretch.

Figure 17 displays flame images using Procedure 1 in the negative process with an air velocity of 30.4 cm/s. The flame displays almost exactly the same cellular structures qualitatively as in the positive process, but those structures did not appear at the same flow conditions. In the negative process, the cells start off as round circles very near the extinction condition. As the flame progressed away from extinction, more cells formed. The burning intensity and flame thickness was almost constant, very much the same as in the positive process. The cells elongate laterally but not in thickness. Also the cells reach a finite length where they can maintain their flatness to the incoming flows and then at that point of time it is preferred by the flame to form a new flat cell of similar length than become concavely curved to the incoming fuel flow [this is seen best in Figure 17 (d) to (e)]. At one flow condition, even if cells differ in length, the distance between cells (length of local flame extinction) is the same. Cells are pushed together in order to form a noncellular flame. Instead of a concave curved flame, two flat flames pushed very close together with a highly curved central area of low burning intensity is seen.

It was shown in the negative process that small flat cells are preferred to long concave curved cells. The burning intensity in the cellular region with flat flames is

stronger than the burning intensity of a concave curved flame. As seen in Table 4, there is hysteresis in cellular formation; the transition from cellular to noncellular occurred at a higher initial mixture strength or lower stretch rate (i.e. higher Damköhler number) in all cases of the negative process than in the positive process. Eventually, that high burning intensity at the flame edges ignited the locally quenched areas and all the flames became noncellular again.

Table 4: Comparison of first cellular state of the positive process with and without mechanical perturbations to the last cellular state of the negative process without mechanical perturbations

	Air Velocity (cm/s)	Φ (1st Cellular State of Positive Process)	Φ (Last Cellular State of the Negative Process)	Φ (1st Cellular State of Positive Process with perturbations)
Procedure 1	30.4	0.469	0.490	0.483
	91.1	0.504	0.538	0.511
Procedure 2	30.4	0.470	0.476	
	91.1	0.517	0.525	
		K (1st Cellular State of Positive Process)	K (Last Cellular State of the Negative Process)	K (1st Cellular State of Positive Process with perturbations)
Procedure 3		261 1/s	190 1/s	230 1/s
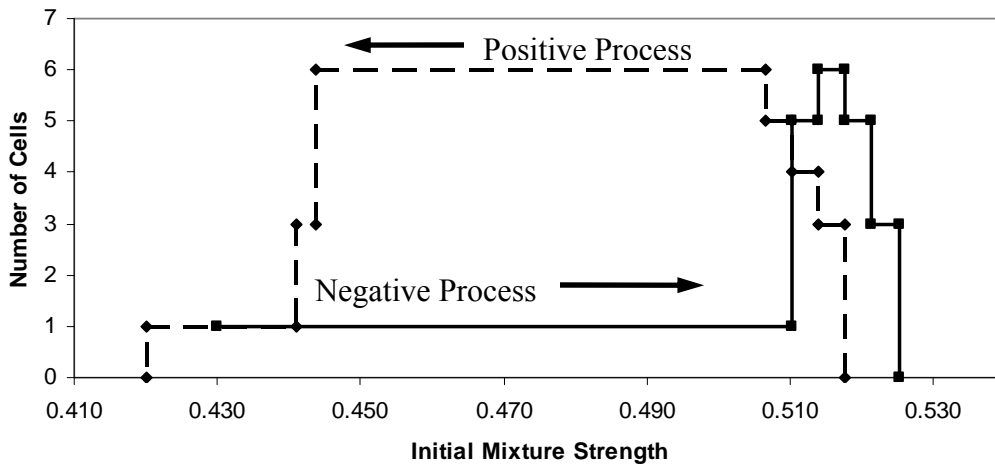
Figure 15: Hysteresis comparison of the number of cells versus the initial mixture strength for the positive process and the negative process using Procedure 2 with air velocity at 91.1 cm/s and K = ~167 1/s. The point of highest initial mixture strength represents the transition from noncellular to cellular for the positive process (or cellular to noncellular for the negative process) and the lowest initial mixture represents the extinction condition. The negative process began at a condition very near the extinction condition. In this test, the flame initially broke at three locations (in the positive process) and the last cellular state in the negative process was also a 3-cell state. 0 cells indicates either extinction or a noncellular flame.
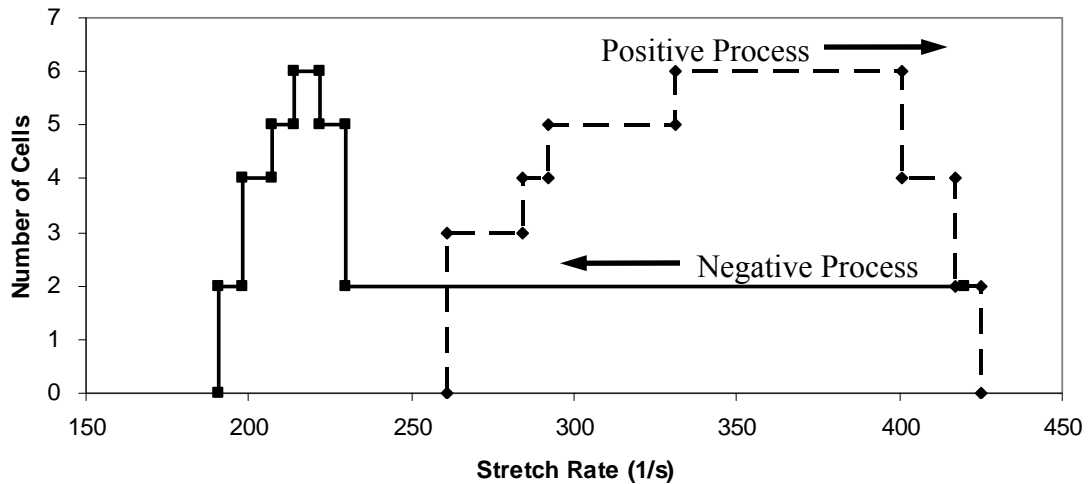
Figure 16: Hysteresis comparison of the number of cells versus stretch rate for the positive process and the negative process using Procedure 3 with $\Phi = 0.518$ and $Le_{fuel} = 0.35$. The point of lowest stretch rate represents the transition from noncellular to cellular for the positive process (or cellular to noncellular for the negative process) and the highest stretch rate represents the extinction condition. The negative process began at a condition very near the extinction condition. In this test, the flame initially broke at three locations (in the positive process) but the last cellular state in the negative process was a 2-cell state. 0 cells indicates either extinction or a noncellular flame.
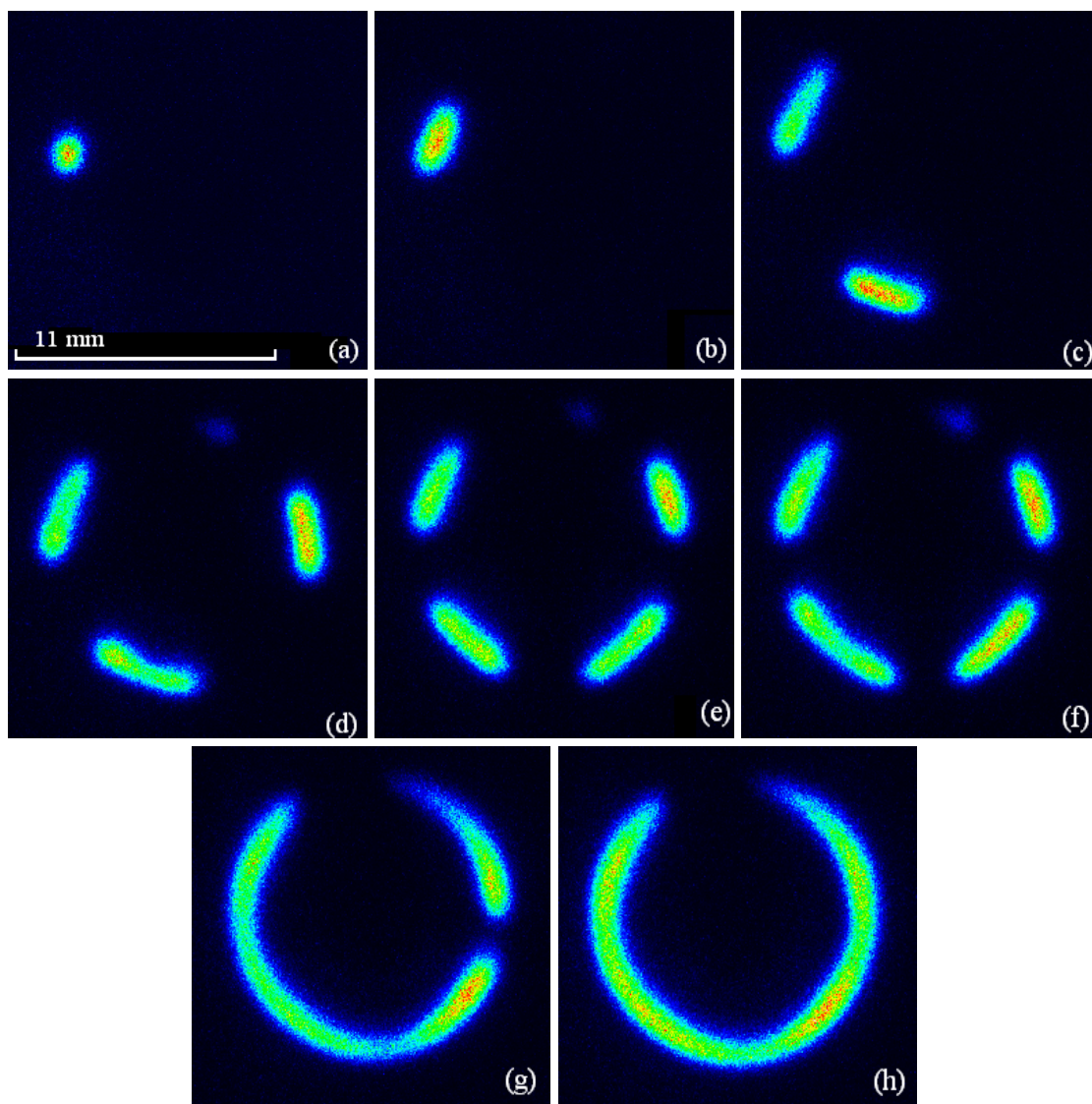
Figure 17: Progression away from extinction with increasing initial mixture strength for opposed tubular flames using Procedure 1 negative process with air velocity at 30.4 cm/s, $K = \sim 86$ 1/s, and $R_s = \sim 5.2$ mm. One cell is obscured by the inner fuel nozzle in (d), (e), and (f). (a) $\Phi = 0.364$, (b) $\Phi = 0.418$, (c) $\Phi = 0.440$, (d) $\Phi = 0.455$, (e) $\Phi = 0.462$, (f) $\Phi = 0.476$, (g) $\Phi = 0.490$, (h) $\Phi = 0.504$

Mechanical Perturbations

Table 5 shows the flow conditions for the positive process with perturbations. Procedures 1 and 3 were conducted again, but this time with perturbations to the flow. Procedure 1: the test began at a condition with a noncellular flame and far from any instability regime. The H_2 flowrate was decreased in steps of .5% of the full scale of the mass flow meter until the flame became extinct. The CO_2 and air flowrates were kept constant. Two of the same oxidizer velocities (30.4 cm/s and 91.1 cm/s) were chosen again to compare these results to previous tests without perturbations. Procedure 3: the test began at a condition with a noncellular flame and far from any instability regime. The air flowrate was increased in steps of 1% of the full scale of the mass flow meter until extinction was realized. The H_2 and CO_2 flowrates were kept constant.

Perturbations to the flow were made using a 1/40 inch (0.635 mm) piece of wire. Unfortunately the wire is a bluff body and not very aerodynamic, therefore the wake around the wire was able to displace almost the entire flame thickness. Tests with metal rods as large as 1/8 inch showed very little difference between the 1/8 inch rod and 1/40 inch wire because almost the entire flame thickness was displaced regardless of perturbation size. This was a good baseline test but more tests need to be conducted with wires of smaller sizes. Unfortunately as the wire decreases in size, the ability to accurately control the perturbation decreases too. A perturbation is defined here as introducing the wire into the reaction zone and then moving the wire a full 360° around the tubular flame in the azimuthal direction until the wire is back to the initial location. Once the perturbation was made, the flame was allowed to stabilize before another perturbation was made. The onset of cellularity was again defined as the condition when

58

two separated cells exist at the same time and extinction was determined when one complete perturbation caused the flame to extinguish.

As can be seen in Table 5, the perturbations have a minimal effect on the onset of cellularity. Looking at Table 4, cellularity was even induced at a lower initial mixture strength or higher stretch rate than in the negative process. This means that the step sizes chosen for the positive and negative process were good values because the momentum perturbation of changing flow conditions was less than that of a mechanical perturbation by a 0.635 mm wire. It was shown that at any condition above the positive transition (noncellular to cellular) a slight perturbation in the negative process caused the negative transition (cellular to noncellular) to occur. Once the flame became cellular, the perturbations had a much increased effect. This was revealed by the ability to induce multiplicity of stable cellular states and to extinguish the flame at a much higher initial mixture strength or lower stretch rate than without perturbations.

Cells were perturbed and the flame became locally extinct at the leading edge of the wire. After the perturbation passed, the area of the flame trailing the wire was reignited and cells grew back quickly. Near extinction, the perturbations had an increased effect on the flame and it became harder for areas of local extinction to become reignited. Very near extinction, perturbations could be done carefully and at flame edge locations of high reactivity in order to reignite or extinguish individual cells. Multiplicity of cellular states was seen and at a wide range of flow conditions it was possible to perturb a flame to a 1, 2, 3, 4, 5, or 6-cell state.

Table 5: Comparison of onset of cellularity and extinction conditions of the positive process with and without mechanical perturbations

	Air Velocity (cm/s)	Conditions at onset of cellularity		Extinction conditions	
		Φ (without perturbation)	Φ (with perturbation)	Φ (without perturbation)	Φ (with perturbation)
Procedure 1	30.4	0.469	0.483	0.356	0.418
	91.1	0.504	0.511	0.440	0.483
		K (without Perturbations)	K (with Perturbations)	K (without Perturbation)	K (with Perturbation)
Procedure 3		261 1/s	230 1/s	425 1/s	331 1/s

CHAPTER V

DISCUSSION

Flame Regimes

While conducting the tests, whether in the negative process or the positive process, there existed three flame regimes. Matalon (2007; 2009) already used the notation of the Damköhler number (Da) to describe flame regimes so that is used here. Da goes from infinity (the fast chemistry limit) where fuel and oxidizer are completely consumed along the stoichiometric surface to Da_{ext} (the extinction limit). As Da approaches Da_{ext} the intensity of the reaction diminishes, the flame temperature drops, and there is leakage of unburned reactants. Extinction occurs when the flame temperature is too low and/or there is excessive leakage of unburned reactants. Within the range $\infty \geq Da \geq Da_{ext}$, there exist two other important Damköhler numbers for cellular flames in the non-premixed opposed-flow tubular burner: Da_{onset} is the condition where the onset of cellularity occurs and $Da_{cellular}$ is the condition during the cellular regime when the maximum number of cells is achieved and after that flow condition the cells are seen to decrease in size and burning intensity. Therefore $\infty \geq Da_{onset} \geq Da_{cellular} \geq Da_{ext}$ is the full region of available Da where $Da_{onset} \geq Da_{cellular} \geq Da_{ext}$ is the region of flame instabilities. The importance of classifying is that each regime displays its own specific traits regardless of using Procedure 1, 2, or 3. A full study of the species concentrations, temperature, and effects of curvature and stretch on flames in the range from

$\infty \geq Da \geq Da_{onset}$ has already been completed (Hu et al., 2009a; Hu et al., 2007; Hu et al., 2009b). Therefore the focus will be on the two regions $Da_{onset} \geq Da \geq Da_{cellular}$ and $Da_{cellular} \geq Da \geq Da_{ext}$. It should be noted that in describing both of these regimes the positive process is used, but these regimes exist in the negative process too (just not at the same flow conditions).

$Da_{onset} \geq Da \geq Da_{cellular}$ is the regime of cellular instability from the onset of cellularity until the flame reaches its maximum number of cells. This regime is very small in Procedures 1 and 2 basically manifesting itself in Figures 10 (b) (Φ=0.469-0.462) and Figure 12 (c) (Φ=0.470-0.464) but it encompasses the progression of Figure 14 (c) to (h) for Procedure 3 (K=261 1/s - 331 1/s). Comparing Figures 15 and 16, the transition from the onset of cellularity until the point when the maximum number of cells was achieved occurred much faster in Procedure 2 than Procedure 3. Therefore, the thinning of the flame to form cells is less sensitive to increasing the stretch rate than decreasing the initial mixture strength. This agrees well with results from planar counterflow diffusion flames, where the flame thickness has been shown to be inversely proportional to the square root of the stretch rate (Sung et al., 1995). Since this regime is significantly larger and displays more interesting features in Procedure 3, Figure 14 will be the focus. Based on chemiluminescence gradients in Figure 14 (c) through (h), in this regime the flame displays varying flame thickness, burning intensity, and curvature. As the stretch is increased, the flame locations of concave curvature display a decreased flame thickness and burning intensity. The areas of most intense burning and thickness are located adjacent to regions of local extinction. The curvature radius of the flame edges is of the same order of magnitude as the flame thickness, so the curvature effect is

very strong at the flame edges. According to Wang et al. (2007), convex curvature towards the fuel strengthens the flame if the Lewis number of the fuel stream is less than one. The flame edges are the strongest part of the flame because of the strengthening effect of preferential diffusion by strong positive curvature. When the strength of the flame edges can no longer support the weak middle section, the cellular flame separates to form smaller cells (smaller in cell length but not in flame thickness). This situation will continue globally around the entire burner until there are no obvious weak middle sections and the cellular flames are completely composed of flame edges, as can be seen in Figure 10 (c), 12 (d), and 14 (h). At this point of time, the flame has reached its maximum number of cells and any decrease in initial mixture strength or increase in stretch rate shortens the cell lengths and moves the flame towards extinction. Also, at this point of time the burning intensity of the flame has gone back to its noncellular burning intensity or even higher at some flow conditions because of the enhanced preferential diffusion by flame curvature.

$Da_{cellular} \geq Da \geq Da_{ext}$ is the regime of cellular instability from when the flame has achieved its maximum number of cells until extinction. This regime is much larger in Procedures 1 and 2 than the regime from the onset of cellularity until the maximum number of cells. The flame images of this regime are seen in Figure 10 (c) to extinction (Φ=0.462-0.356), Figure 12 (d) to extinction (Φ=0.464-0.298), and Figure 14 (h) to extinction (K=331 1/s - 425 1/s). As the stretch rate is increased in Figure 14, the flame moves closer to the inner fuel nozzle and extinction can be partially caused by heat loss to the burner. Therefore in this regime focus should be put on Figures 10 and 12 and not as much on Figure 14. As can be seen in Figures 10 and 12, once the maximum number

of cells is formed, the flame no longer displays any significant chemiluminescence gradient in each individual cell. The middle section of the flame cell is completely flat to the incoming fuel flow. The burning intensity is unchanged until very near extinction. The flame thickness decreases but only slightly. Most importantly is the decrease in flame length (as seen best in Figure 10). As the cells decrease in length, cells that were once very different in length eventually become circular flames with relatively the same flame thickness (or flame diameter as they become circular). This further confirms the fact that the positively curved flame edges strengthen the preferential diffusion. Another feature of these flame images is the spacing between cells (i.e. the regions of local flame extinction). At one flow condition, even if cells differ in length, the distance between cells (length of local flame extinction) is almost the same. This is best seen in Figure 12 (d), as it is clear that the cells all differ in length but the regions of local extinction are of very similar size. This phenomenon only fails very near extinction when cells begin to extinguish. It is believed that the cells act as one until the first cell extinguishes, then the cells act as individual entities. This has been shown numerically by Lee and Kim (2002).

Flame Rotation

Lo Jacono et al. (2003) first saw a cellular flame rotate in a non-premixed AJ burner. It was shown that a 1-cell, 2-cell, and 3-cell state were all seen to rotate; and that rotation was in both the clockwise and counterclockwise direction. In a non-premixed opposed-flow tubular burner, Hu et al. (2009a) saw a 1-cell flame rotate and rotation was seen in both the clockwise and counterclockwise direction too. Valär et al. (2010) modeled the AJ burner of Lo Jacono et al. (2003) and Lo Jacono and Monkewitz (2007)

and numerically displayed 3-cell flame rotation. Individual cells were never in continuous motion. One cell was seen moving as the others were stationary. The cell in motion was shown to have a leading edge of high reactivity adjacent to a locally quenched region where partial premixing was occurring. Valär et al. (2010) calculated the flame index (level of premixing) and found that there was partial premixing along the cellular flame edges and in the regions of local extinction between cells. Even though these simulations were done in an AJ burner, this type of cellular movement is very similar to what has been seen experimentally in the non-premixed opposed-flow tubular burner of this study.

Figure 18 displays a top view of a rotating cellular flame. Rotation is counterclockwise and the time interval between consecutive images is ~70 ms. Figure 19 displays a side view of rotating cellular flames. Rotation is from left to right and the time interval between consecutive images is ~60 ms. It can be seen in Figure 18 (a), rotation is initiated at the positively curved flame edge in cell 1. Cell 1 begins to elongate and in doing so becomes more concavely curved. In order to keep a consistent distance between cells, as cell 1 elongates it pushes cells 2 and 3 in the counterclockwise direction [cell 3 eventually combines with cell 4, Figure 18 (c)]. When cell 1 elongates to an extent that it has developed a weak middle section [Figure 18 (d)], the strong burning end breaks off and begins to move counterclockwise [Figure 18 (e)]. The original cell 1 remains stationary. Now cell 2 is forced to move counterclockwise and eventually combines with cell 4 [Figure 18 (g)]. Throughout the whole process, cells 1 and 4 have remained stationary.

Rotation in this burner is seen with a high number of cells, which is different from the 1-cell flame rotation in Hu et al. (2009a). This is probably caused because the

previous tubular burner in Hu et al. (2009a) was of a larger size and realized much lower stretch rates and curvature than this burner. The 1-cell flame rotation in Hu et al. (2009a) occurred at a stretch rate of 73 1/s whereas the stretch rates of this study go from 88 1/s to 425 1/s (Table 1).

It has been shown in premixed flames by Sakai and Ishizuka (1992) that the flammability range shifts towards the fuel lean side for methane and fuel rich side for propane when comparing a tubular flame in a rotating versus non-rotating flow field. It was believed that the rotating flow field aided the stratification of the fuel by preferential diffusion and the flammability range was extended by the effect of curvature and the rotating motion of the mixture. In a follow-up study, Yamamoto et al. (1994) further investigated the effects of rotation on premixed tubular flames and showed that increasing the rotational intensity decreased the lean flammability limit of methane and raised the flame temperature even though the OH concentration was shown to decrease. This phenomenon was attributed to a mechanism similar to that of an excess enthalpy flame.

Rotation in this burner is achieved through movement initiated near a positively curved flame edge displaying high reactivity adjacent to a partially premixed region of local extinction. Rotation is mainly seen from $Da_{onset} \geq Da \geq Da_{cellular}$, which has the highest initial mixture strengths and the lowest stretch rates of the cellular regime. The higher initial mixture strength means that there is available hydrogen in the flow field for premixing and the fact that the flame is rotating means that the flammability limit is decreased to a leaner value than that of a nonrotating flame. Low stretch rates mean that the flame has enough time to diffusion laterally in the direction of the reaction zone

66

against the convective flow normal to the flame. Therefore it is believed that partial premixing (even very lean partial premixing conditions) in the locally quenched areas near strong flame edges induce rotation. At high stretch rates and low initial mixture strengths, the flame is not seen to rotate. Premixing and flame edges of high reactivity can occur at any location on the flame, this explains the fact that rotation was seen in either the clockwise or counterclockwise direction.
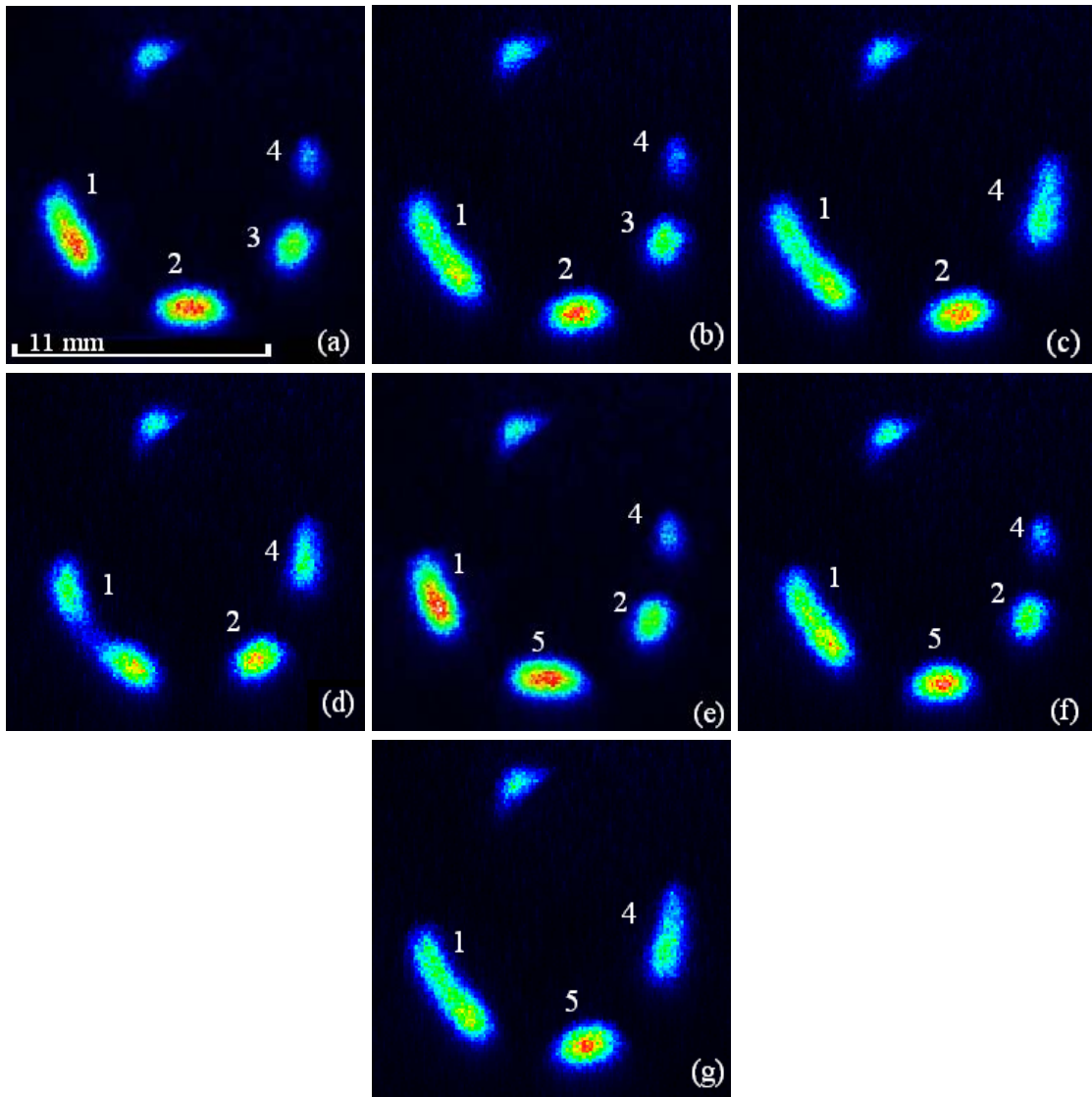
Figure 18: Top view displaying rotating cellular flames versus time with Φ=0.448 and K= 88 1/s. Inner fuel nozzle is partially obscuring backside of flame. Rotation is counterclockwise (e.g. cell 2, 3, and 5) and the time interval between consecutive images is ~70 ms.

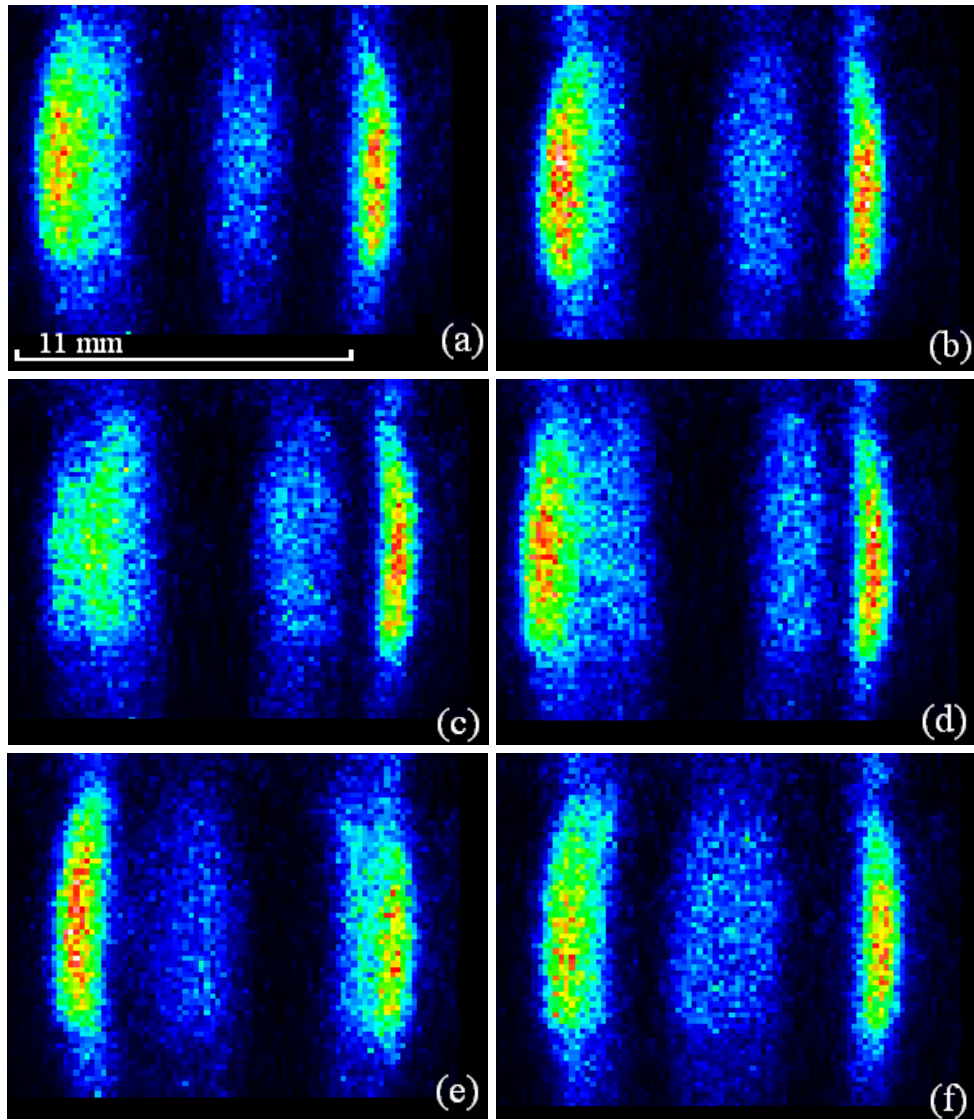Figure 19: Side view displaying rotating cellular flames with Φ=0.455 and K= 88 1/s. Inner fuel nozzle is not shown. The two outer cellular flames appear to have higher burning intensities because from this angle those flames are several millimeters thick and the middle cellular flame is roughly ~1 mm thick. Rotation is from left to right and the time interval between consecutive images is ~60 ms.

Comparison of Extinction by Initial Mixture Strength

A final comparison was made between approaching extinction using Procedures 1 and 2. Figure 20 displays the results of both of these procedures. As can be seen in Figure 20, in all tests Procedure 1 caused the flame to extinguish at a lower stretch rate and a higher initial mixture strength than Procedure 2. What needs to be remembered is that Procedure 2 moves the flame away from the inner fuel nozzle reducing the flame curvature and heat loss to the burner. Figure 21 shows the same data as Figure 20, except now the abscissa is the stagnation radius. As can be seen in Figure 21, increasing the stagnation radius allows the cellular flame to remain flammable until higher stretch rates and lower initial mixture strengths. When the difference in stagnation radius between Procedures 1 and 2 is decreased, the extinction condition is almost the same. It should be noted that Procedure 1 started losing cells at a higher initial mixture strength and lower stretch rate in all tests too. This comparison shows the strength curvature has on preferential diffusion, specifically concave curvature towards the fuel suppressing cellular instability. This agrees well with previous experimental results (Hu et al., 2009a). It is interesting to note in Figure 21, that regardless of the stagnation radius, the onset of cellularity is a fairly rigid condition. This was also seen in the case of mechanical perturbations (Table 3).

Figure 20: Comparison of the flow conditions at the onset of cellularity and extinction versus stretch rate for the positive process Procedure 1 (♦) and positive process Procedure 2 (■). Highest point of each line (highest initial mixture strength) is onset of cellularity and lowest point of each line (lowest initial mixture strength) is extinction condition.
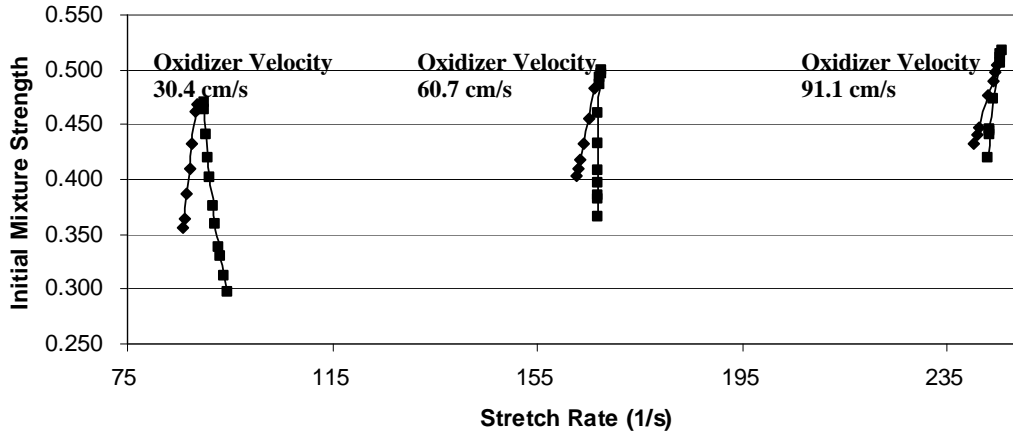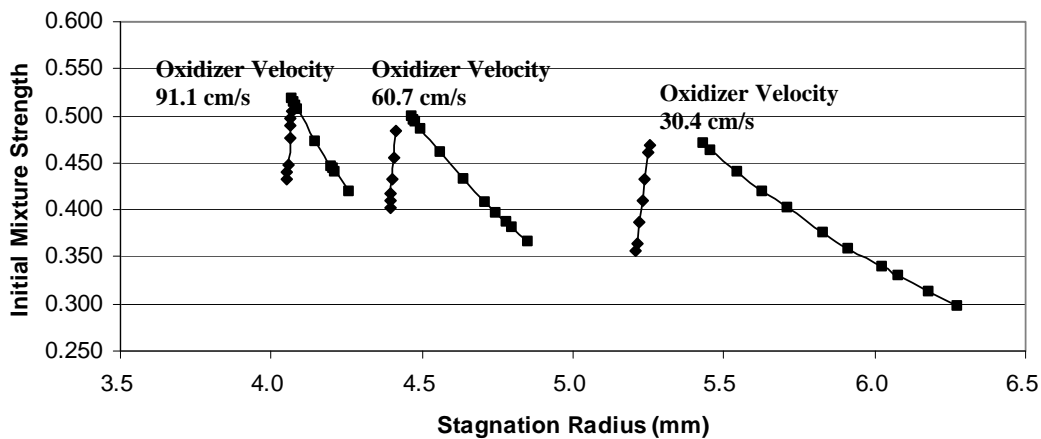

Figure 21: Comparison of the flow conditions at the onset of cellularity and extinction versus stagnation radius for the positive process Procedure 1 (♦) and positive process Procedure 2 (■). Highest point of each line (highest initial mixture strength) is onset of cellularity and lowest point of each line (lowest initial mixture strength) is extinction condition.

Flames Stabilized on Inner Fuel Nozzle

One last experiment was conducted to test the effect of heat loss to the inner nozzle. Procedure 2 was conducted again with the air velocity of 60.7 cm/s, but this time in the negative process. The test began at a condition very near the extinction limit (cellular flame) and then the CO_2 flowrate was decreased in steps of .333% of the full scale of the mass flow meter until the flame became noncellular. The H_2 and air flowrates were kept constant. Once the flame became noncellular, instead of stopping the test, the CO_2 flowrate was decreased even more and eventually the flame became cellular again. This was the only test where a 7-cell flame was seen, the highest number of cells before this test was only 6-cells even with perturbations. Lowering the CO_2 flowrate even more, the flame became stabilized on the inner fuel nozzle. Figure 22 shows the images of the flame cells stabilized on the inner fuel nozzle. Figure 22 (d) looks different than the others because at that condition it was a pure hydrogen/air flame with no CO_2 diluting the flow.

Figure 22 shows that it was possible for a cellular flame to stabilize on the inner fuel nozzle. This added another flame regime unseen in other tests. This test was conducted three times with the same results each time. It was not conducted under other conditions because the fuel nozzle is not constructed to withstand flames on its surface. Therefore no more testing was done. This last test was unable to quantify the heat loss to the inner fuel nozzle, but it displayed a new cellular regime unseen before now in this non-premixed opposed-flow tubular burner. Cellular instability was displayed at an initial mixture strength greater than unity and away from extinction conditions but subject to heat loss at the burner surface.
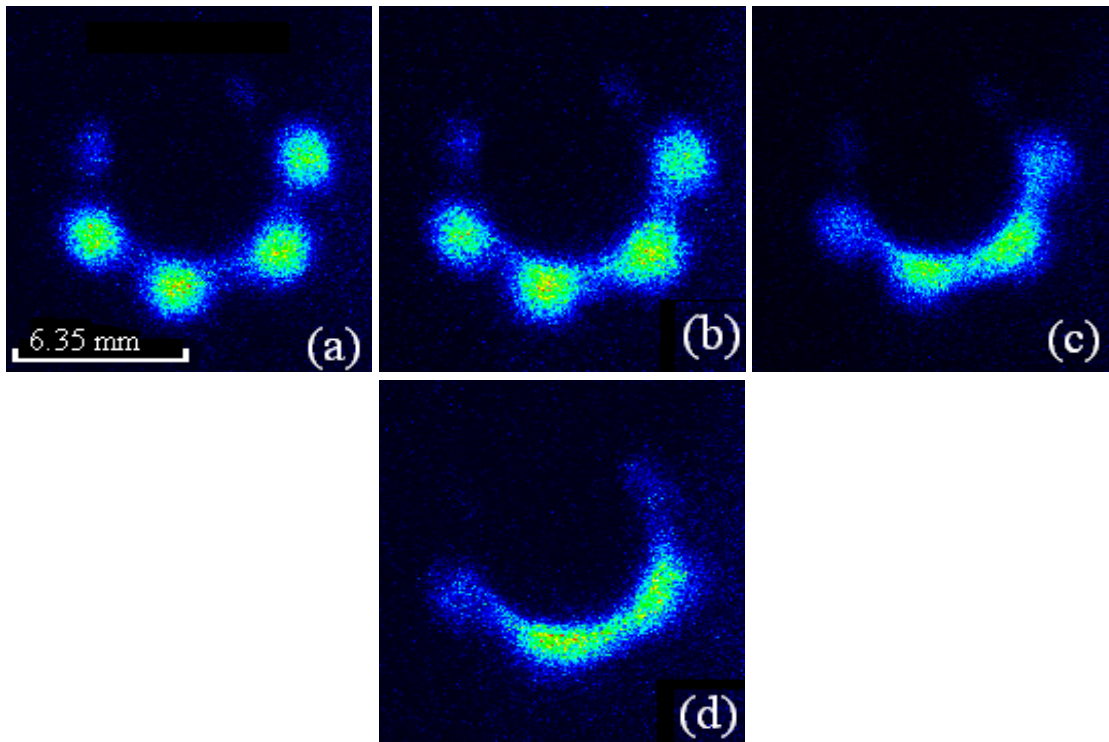
Figure 22: Cells stabilized on the inner fuel nozzle. 7 cells were stabilized with 3 being obscured by the inner fuel nozzle. (a) Φ=1.587, (b) Φ=1.786, (c) Φ=2.041, (d) Φ=2.381

<u>Cellular Formation and Flame Thinning</u>

Figure 23 shows in more detail the effects of stretch on tubular diffusion flames and displays the formation of cells in these flames. The flame images are taken from Figure 6 and the number and letter is given in the caption. To form the cellular flame structure, there are two conditions that must be satisfied: 1) the noncellular flame has to be weak and close to the onset of cellularity. Only when the flame is weak enough, can a perturbation form a location of local flame extinction. Also, sometimes the gap between two cellular flames can be reignited after the perturbation is gone if the flame edges are strong enough. Strong edge flames near areas of local extinction can be seen in Figure 6 (b). Lateral re-ignition of certain quenched areas near strongly burning edge flames has been seen experimentally in the non-premixed opposed-flow tubular burner of this study and numerically by Valär et al. (2010). 2) After the local extinction, the formed cellular flame has to be stronger than the original noncellular flame or else the whole flame would be extinguished. This is seen in Figure 6 (c). The cellular flame that exists between two areas of local extinction displays a higher burning intensity than the rest of the concave curved flame. After the noncellular flame is extinguished locally, a cellular flame is formed. This cellular flame has a chemiluminescence gradient in the azimuthal direction which indicates a temperature gradient throughout the cell in that direction (the perfect tubular flame only has gradients in the radial direction). The edges of the cellular flame are at a significantly higher temperature than the cell's midsection. In this structure, the edges enhance the flame and the center acts as a heat sink. The flame edges are positively curved to both the oxidizer and fuel streams. It was shown by Hu and Pitz

(2009) for H_2 diluted in N_2 versus air flames that convex curvature could raise the flame temperature 100-200 Kelvin over concave curvature at the same flow conditions.

The curvature radius of the flame edges is of the same order of magnitude as the flame thickness, so the curvature effect is very strong at the flame edges. According to Wang et al. (2007), convex curvature towards the fuel enhances the flame if the Lewis number of the fuel stream is less than one. This is the case for the edge flame and the cellular flame is stronger than the noncellular flame because of the strengthening effect of preferential diffusion by strong positive curvature of the flame edges. When the strength of the flame edges can no longer support the weak middle, the cellular flame separates to form smaller cells (smaller in cell length but not in flame thickness). This situation will continue globally around the entire burner until there are no obvious weak middle flames and the cellular flames are completely composed of flame edges, as can be seen in Figure 6 (h) and (i). Seen in Figure 6 (f), as edge flames form they resist concave curvature altogether and become flat to the incoming fuel flow. This resistance to concave curvature strengthens the preferential diffusion of the fuel. The strength of the edge flames comes from the preferential diffusion of the fuel and the strong positive curvature of the edge flames. Further increase of the stretch rate will shrink the edge flames laterally until the flames become circular, as seen in Figure 6 (i). Flame extinction occurs when the flame edges can no longer support themselves.

To illustrate the strength of the convex flame edges, the following comparison was made. Using the cellular images of Figure 8, the full width half max (FWHM) flame thickness, δ, based on the chemiluminescence from the flame was measured and graphed versus the inverse of the square root of the stretch rate. It has been well documented by

75

Sung et al. (1995) that planar diffusion flames become thinner with increasing the stretch rate; they found the flame thickness varies as $\delta \sim 1/\sqrt{K}$. Figure 24 shows a graph of this phenomenon. The edge thickness stays the same throughout the course of increasing stretch. The two newly separated edge flames shown in Figure 8 (f) were actually slightly thicker than the corresponding edge flames in Figure 8 (a) even though the stretch rate was increasing from Figure 8 (a) to (f). This further shows that the weak center acts as a heat sink to the flame edges as the convex edge flame to the fuel is able to increase in thickness (slight as it is) once the center becomes locally extinct. The center flame thickness decreases with stretch similar to planar diffusion flames following the dependence $\delta \sim 1/\sqrt{K}$.

It is interesting to note that in the recent numerical study by Valär et al. (2010), the region of the flame convex to the limiting reactant (hydrogen) displayed an increased heat release rate. This was explained by the preferential diffusion of the fuel compared to the diffusion of heat. Also in that same study, it was numerically feasible to simulate cells of differing sizes and burning intensities. The largest cells displayed the lowest temperatures and this was explained by the fact that these cells possessed the smallest ratio of surface area towards the limiting reactant (hydrogen) to cell volume. This is very similar to what has been observed experimentally in the non-premixed opposed-flow tubular flames, where convex curvature towards the limiting reactant displayed an increased burning intensity over the concave curved flames and cells of differing sizes and burning intensity were seen throughout the flame. It will be important in the future to be able to predict using numerical simulations the flame edge thickness as well as the temperature gradient within the cellular structures of the tubular flames.
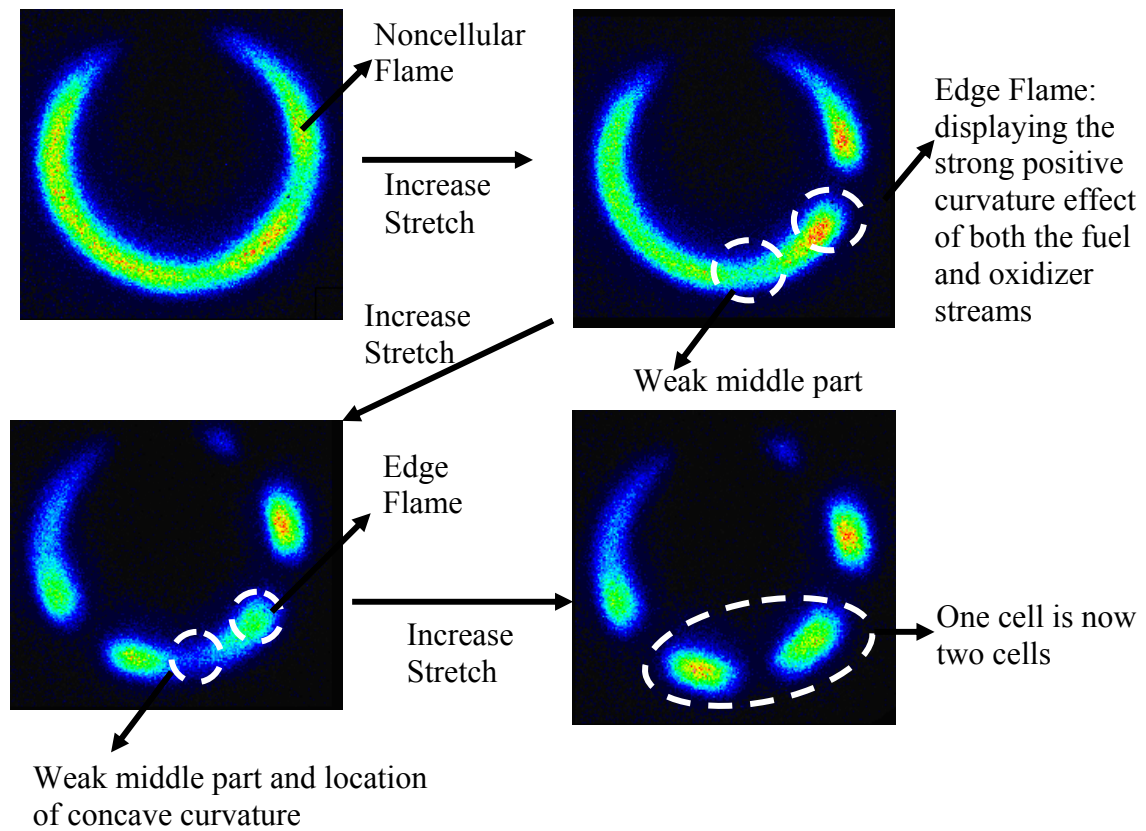
Figure 23: Schematic of one cell becoming two cells as stretch rate increases in 21.7% H_2 diluted with CO_2 versus air opposed tubular flames. Flame images come from Figure 6 (clockwise from upper left): 6 (a), 6 (b), 6 (f), and 6 (e)
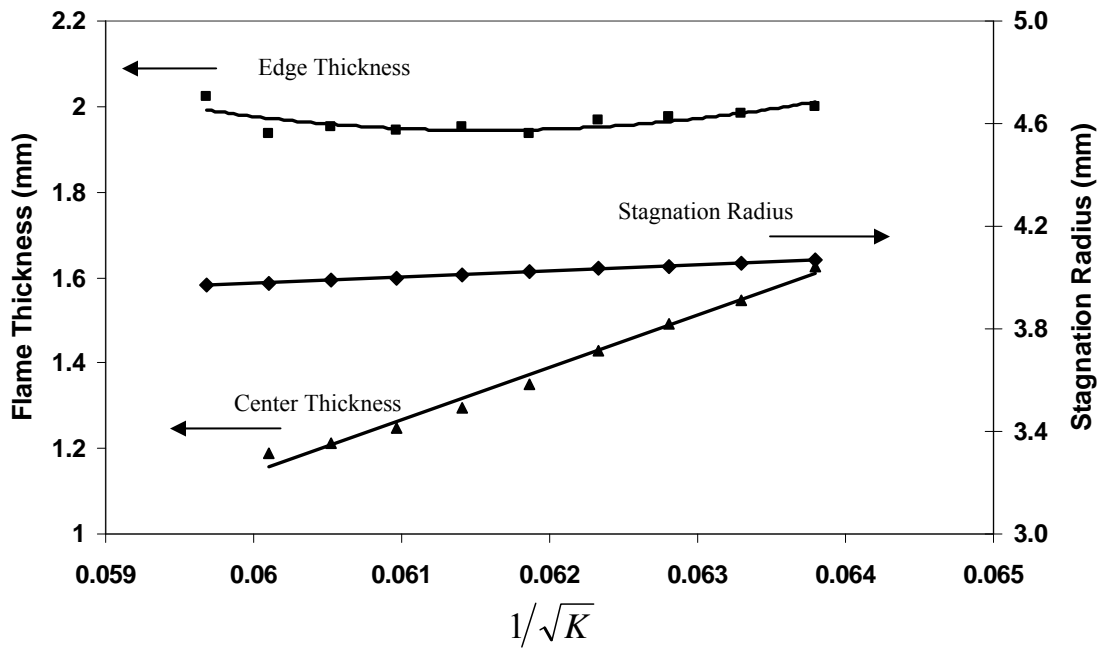
Figure 24: Measured flame thickness and calculated stagnation radius versus square root of inverse of the calculated stretch rate for 21.7% H_2 diluted in CO_2 versus air opposed tubular flames

CHAPTER VI

CONCLUSIONS

Cellular formation in non-premixed stretched, curved flames is studied experimentally in the opposed-flow tubular burner with an inner nozzle flowing fuel (H_2 diluted with CO_2) and an outer nozzle flowing air. The global stretch rate and overall flame curvature can be varied independently in this burner unlike other flame geometries. The chemiluminescence emission from the cellular flames is imaged onto an intensified CCD camera. Cells are formed at low reactant Lewis numbers, low initial mixture strengths, and near extinction conditions. The cellular instabilities are found to form at or above the numerically calculated 1D extinction limit of the opposed tubular flame. For fuel Lewis numbers less than unity, concave curvature toward the fuel retards combustion and weakens the cellular structures whereas convex curvature toward the fuel (specifically at the flame edges) promotes combustion and strengthens the cellular structures. With the low Lewis number fuel emanating from the inner nozzle, the flame cell midsection which displays strong concave curvature is weaker than the cell ends which display convex curvature. With increasing the stretch rate, the cell breaks and this cell formation process continues until the flame cells are near circular with no concave midsection. Further increase in stretch rate leads to cellular flame extinction. It is found that the cell midsection thickness decreases with stretch rate similar to planar diffusion flames. However, the edge flame thickness is constant or slightly increases with stretch rate due to the strengthening effect of convex curvature. These results illustrate the

importance of local flame curvature in the formation of cellular flames and in the existence of cellular flames well beyond the 1D extinction limit.

A further experimental study was conducted in flames burning H_2 diluted with CO_2 flowing against air. Cells formed at low reactant Lewis numbers of the fuel, low initial mixture strengths, and near extinction conditions except in the case of cellular instability stabilized on the inner fuel nozzle. In that case, it was possible to display cellular structures at initial mixture strengths greater than unity and away from extinction conditions. It has been shown that transitioning the flame towards extinction (positive process) or away from extinction (negative process) displays significant hysteresis. It was shown that the transition from a noncellular to cellular flame occurred at a lower initial mixture strength or higher stretch rate (i.e. lower Damköhler number) in the positive process than the negative process. It was also shown that it was always feasible for a cellular flame to return to a noncellular flame.

Mechanical perturbations to the flow proved that the onset of cellularity could not be affected significantly but it was feasible to extinguish the flame at a much higher initial mixture strength or lower stretch rate with perturbations than without perturbations. It was also shown that it was possible to induce multiple stable cellular states at the same condition by mechanical perturbations.

Observing the flame images, it was possible to view the chemiluminescence gradients in the flame which correspond to gradients in the burning intensity (i.e. temperature). To the authors' knowledge, this is the first time that experimental non-premixed cellular flame images of this clarity and detail have been seen. Images are

shown of rotating cellular flames too. Lastly, a qualitative explanation of flame rotation and a general categorizing of three distinct flame regimes are given.

Future Efforts

There exist numerous future efforts and experiments that can still be conducted in the NPOF tubular burner at Vanderbilt University to help combustion researchers better understand flame instabilities. A first effort would be to improve the burner's flow field. In order to accomplish this, it would be necessary to fill in the optical access ports with a steel wool like material and place aluminum tape over the holes. It was noticed that the initial locations of weak burning or local extinction in both Procedures 1 and 2 (Figures 10 and 12, respectively) were at the optical access ports. While these ports do provide side views of the flame, their affect on the flow field inside the burner is noticeable. A second improvement to the burner would be to improve the inner fuel nozzle. The Mott Corporation is now making porous cylinders of Hastelloy. The Hastelloy material would be able to withstand greater flame temperatures before failure (failure would be when the material was stressed to the point that it created an imperfect flow field). All the current inner fuel nozzles have a finite lifetime before they are "burnt out". More experiments with flames sustained on the burner surface could be conducted too. Also, it would be beneficial to have a new inner fuel nozzle of a smaller radius so that heat loss to the burner was decreased or eliminated altogether.

Besides improvements to the NPOF tubular burner, there are additional experiments that could be conducted. Comparisons have already been made on flame temperature, thickness, flammability limits, etc. between planar and curved diffusion

flames; yet more comparisons could be researched and conducted. One easy comparison would be to measure the flame thickness versus the stretch rate, $\delta \sim 1/\sqrt{K}$, once the flame has reached its maximum number of cells for Procedure 3. This analysis was accomplished and a correlation was made for the weak middle sections (concave curved flames) but only while the flame was breaking up into cells. It would also be interesting to see a correlation between flame lengths versus the initial mixture strength for Procedures 1 and 2. It has been shown that the flame length decreases with decreasing initial mixture strength, maybe a simple mathematical correlation exists? Raman measurements of flame temperature and species concentrations have already been accomplished in tubular flames but only in the noncellular regime. It would be interesting to perform Raman measurements in the cellular regime too. Lastly, it has been shown how inaccurate the 1D numerical simulations are. There exists a definite need to improve these techniques in order to display the complex 3D cellular structures. Experimental results exist, now numerical simulations need to be performed.

REFERENCES

Brown, T.M., M.A. Tanoff, R.J. Osborne, R.W. Pitz, and M.D. Smooke (1997), "Experimental and Numerical Investigation of Laminar Hydrogen-Air Counterflow Diffusion Flames," *Combust. Sci. and Tech.* **129**, p. 71.

Cheatham, S., and M. Matalon (2000), "A General Asymptotic Theory of Diffusion Flames with Application to Cellular Instability," *J. Fluid Mech.*, **414**, p. 105.

Chen, R.H., G.B. Mitchell, and P.D. Ronney (1992), "Diffusive-Thermal Instability and Flame Extinction in Non-Premixed Combustion." 24th Symposium (Int.) on Combustion, The Combustion Inst, p. 213.

Hu, S., P. Wang, R.W. Pitz, and M.D. Smooke (2007), "Experimental and Numerical Investigation of Non-Premixed Tubular Flames," *Proc. Combust. Inst.*, **31**, p. 1093.

Hu, S., and R.W. Pitz (2009), "Structural Study of Non-Premixed Tubular Hydrocarbon Flames," *Combust. Flame*, **156**, p. 51.

Hu, S., R.W. Pitz, and Y. Wang (2009a), "Extinction and Near-Extinction Instability of Non-Premixed Tubular Flames," *Combust. Flame*, **156**, p. 90.

Hu, S., P. Wang, R.W. Pitz (2009b) "A Structural Study of Premixed Tubular Flames," *Proc. Combust. Inst.*, **32**, p. 1133.

Ishizuka, S. (1993), "Characteristics of Tubular Flames," *Prog. Energy Combust. Sci.*, **19**, p. 187.

Karlovitz, B., D.W. Denniston, D.H. Knapschaefer, and F.H. Wells (1953), "Studies on Turbulent Flames," 4th Symposium (Int.) on Combustion, The Combustion Inst, p. 613.

Kim, J.S., F.A. Williams, and P.D. Ronney (1996), "Diffusional-Thermal Instability of Diffusion Flames," *J. Fluid Mech.*, **327**, p. 273.

Law, C.K. (1988), "Dynamics of Stretched Flames," 22th Symposium (Int.) on Combustion, The Combustion Inst, p. 1381.

Lee, S.R., and J.S. Kim (2002), "On the Sublimit Solution Branches of the Stripe Patterns Formed in Counterflow Diffusion Flames by Diffusional-Thermal Instability," *Combust. Theory Modelling*, **6**, p. 263.

Lo Jacono, D., P. Papas, and P.A. Monewitz (2003), "Cell Formation in Non-Premixed, Axisymmetric Jet Flames Near Extinction," *Combust. Theory Modelling*, **7**, p.635.

Lo Jacono, D., P. Papas, M. Matalon, and P.A. Monkewitz (2005), "An Experimental Realization of an Unstrained Planar Diffusion Flame," *Proc. Combust. Inst.,* **30**, p. 501.

Lo Jacono, D., and P.A. Monkewitz, (2007), "Scaling of Cell Size in Cellular Instabilities of Nonpremixed Jet Flames," *Combust. and Flame*, **151**, p. 321.

Matalon, M. (1983), "On Flame Stretch," *Comb. Sci. Technol*., **31**, p. 169.

Matalon, M. (2007), "Intrinsic Flame Instabilities in Premixed and Nonpremixed Combustion," Annu. Rev. Fluid Mech., **39**, p. 163.

Matalon, M. (2009), "Flame Dynamics," *Combust. Flame*, **32**, p. 57.

Peters, N. (1984). "Laminar Diffusion Flamelet Models in Non-Premixed Turbulent Combustion." *Prog. Energy Combust. Sci.,* **10**, p. 319.

Robert, E., and P.A. Monkewitz (2009), "Experiments in a Novel Quasi-1D Diffusion Flame with Variable Bulk Flow," *Proc. Combust. Inst*., **32**, p. 987.

Sakai, Y., and S. Ishizuka (1992), "Extinction Characteristics of Tubular Flames Diluted with Nitrogen in a Rotating Stretched Flow Field." 24th Symposium (Int.) on Combustion, The Combustion Inst, p. 153.

Seshadri, K., and F.A. Williams (1978) Int. J. Heat Transfer, **21**, p. 251.

Shay, M.L., and P.D. Ronney (1998), "Non-Premixed Edge Flames in Spatially Varying Straining Flows," *Combust. Flame*, **112**, p. 171.

Sung, C.J., J.B. Liu, and C.K. Law (1995), "Structural Response of Counteflow Diffusion Flames to Strain Rate Variations," *Combust. Flame*, **102**, p. 481.

Valär, A.L., C.E. Frouzakis, P. Papas, A.G. Tomboulides, and K. Boulouchos (2010), "Three-Dimensional Simulations of Cellular Non-Premixed Jet Flames," *Combust. Flame*, **157**, p. 653.

Wang, P., S. Hu, and R.W. Pitz (2007), "Numerical Investigation of the Curvature Effects on Diffusion Flames," *Pro. Combust. Inst.*, **31**, p. 989.

Wang, P., J.A. Wehrmeyer, and R.W. Pitz (2006), "Stretch Rate of Tubular Premixed Flames," *Combust. Flame,* **145**, p.401.

Wang, Y., S. Hu, and R.W. Pitz (2009), "Extinction and Cellular Instability of Premixed Tubular Flames," *Proc. Combust. Inst.,* **32**, p. 1141.

Williams, F.A. (1975) A review of some theoretical considerations of turbulent flame structure, in: AGARD Conference Proceedings No. 164, Paris, pp. II 1-25.

Yamamoto, K., S. Ishizuka, and T. Hirano (1994), "Effects of Rotation on the Stability and Structure of Tubular Flame." 25th Symposium (Int.) on Combustion, The Combustion Inst, p. 1399.